Spatiotemporal signaling dynamics evoked by single binding interactions between a peptide-bound MHC molecule and a T cell receptor

By

Darren McAffee

A dissertation submitted in partial satisfaction of the

requirements for the degree of

Doctor of Philosophy

in

Chemistry

in the

Graduate Division

of the

University of California, UC Berkeley

Committee in charge:

Professor Jay Groves, Chair
Professor Jeremy Thorner
Professor David Wemmer

Fall 2019

Spatiotemporal signaling dynamics evoked by single binding interactions between a peptide-bound MHC molecule and a T cell receptor

Abstract

Spatiotemporal signaling dynamics evoked by single binding interactions between a peptide-bound MHC molecule and a T cell receptor

By

Darren McAffee

Doctor of Philosophy in Chemistry

University of California, Berkeley

Professor Jay Groves, Chair

T cells (TCs) have the crucial immunological task of discriminating foreign peptide fragments from endogenous (self) peptide fragments. This recognition is carried out by the T Cell Receptor (TCR) on the TC surface, which binds to an antigen-derived peptide fragment presented by major histocompatibility complex (pMHC) on the surface of an Antigen Presenting Cells (APC). Despite the centrality of this TCR:pMHC interaction and the myriad techniques used analyze it, few studies exist in which the signaling consequences of individual TCR:pMHC binding events have been determined. Direct examination of the outcomes from single TCR:pMHC encounters provides insight into how the stochastic signaling network of the T cell performs crucial tasks such as signal integration and ligand discrimination. In Chapter 1, individual TCR:pMHC binding interactions (dwell times) are mapped to two proximal events in T cell activation: the assembly of Linker for Activation of T cells (LAT) molecules; and, translocation of Nuclear Factor of Activated T cells (NFAT). After TCR engagement with agonist pMHC, the LAT scaffold protein forms a hub of signaling from which a number of subsequent signaling steps are initiated; hence, LAT assembly is a gatekeeper of downstream signaling. I observe that the probability of LAT assembly formation, localized to ligated TCR, is an increasing function of the dwell time of the TCR:pMHC interaction, suggesting that the formation of LAT assembly from ligated TCR represents a form of kinetic proofreading; however, the size and lifetime of a LAT assembly is independent of the TCR:pMHC dwell time interaction that produced it. This discreteness of LAT clustering from TCR:pMHC dwell time has consequences for signal integration from multiple binding events. In Chapter 2, I explore what distinguishes a productive TCR:pMHC binding event from one that fails to trigger LAT assembly, as an approach to delineate the “kinetic bottlenecks” in antigen discrimination and T cell activation. I found that activation of zeta-chain-associated protein kinase of 70 kDa (ZAP-70), which phosphorylates LAT at multiple sites, is necessary, but insufficient. Aside from ZAP-70 activity, diffusive phospho-LAT requires an additional event to trigger aggregation. Importantly, I found that, at low pMHC densities, PLC-γ1 controls the timing for the initiation of LAT clustering, a

dependency not previously identified. One feature I readily observed in my experiments is that LAT assemblies can form without any apparent originating pMHC. The composition and function of these apparent orphan LAT assemblies are investigated preliminarily in Chapter 3. In summary, by measuring the correlation between single receptor (TCR)-ligand (pMHC) binding events and subsequent steps in T cell activation, one obtains unprecedented quantitative insight into the stochastic nature of signal transduction in T cells.

Table of Contents

Table of Figures

Acknowledgements

Thank you Dad, for your lessons

Thank you Mom, for your love

Thank you Teachers, for your clarity

1 | Localized LAT condensation phase transitions discriminate individual TCR:pMHC binding dwell times.

Abstract

The process of antigen discrimination by T cells is essential for a correct immune response. This process is initiated by an agonist-pMHC ligand binding to a T cell receptor (TCR). A crucial step downstream of binding is the formation of an extended multi-molecular protein condensate that is crosslinked by the Linker for Activation of T cells (LAT) protein. However, techniques to analyze how individual pMHC-TCR binding events produce these LAT condensates have been lacking. Here, we image single pMHC-TCR binding events and map them to the condensation of LAT with other downstream molecules. A supported lipid bilayer (SLB) is functionalized with adhesion molecules and fluorescent agonist pMHC. T cells are then introduced to the bilayer and pMHC-TCR binding events are distinguished from free pMHC by their dramatic change in diffusivity. An isolated long-dwelling binding event is regularly observed to be sufficient for producing a localized transient burst of LAT condensation. Quantification of the condensates reveals that TCR:pMHC dwell-time is transduced in a digital manner. Many binding events fail to produce LAT assemblies, but the likelihood of localized LAT condensation increases with TCR:pMHC dwell time. Furthermore, as multiple distinct LAT condensates are produced, they are capable of integrating signal to trigger T cell activation. In summary, we find that the antigen discrimination process at the single-molecule level involves condensation of LAT and that these transient condensates may be basic units of signal integration within T cell activation.

Introduction

A healthy adaptive immune response depends on the ability of T cells to discriminate between agonist peptide major histocompatibility complex (agonist-pMHC) ligands and the vastly more abundant self-pMHC. It has long been recognized that antigen discrimination depends strongly on the binding kinetics of pMHC to T cell receptor, especially the kinetic off-rate (Daniels et al., 2006; Matsui et al., 1994; Robert et al., 2012). This task is complicated by the fact that agonist and self-ligands may differ only slightly in their binding kinetics (Corr et al., 1994), requiring a highly precise discrimination mechanism (McKeithan, 1995). Furthermore, T cells must accurately discriminate pMHC ligands based on less than tens of agonist pMHC being present at the APC:TC interface (Delon et al., 1998; Demotz et al., 1990; Harding and Unanue, 1990; Huang et al., 2013).

Signaling from triggered TCR proceeds via the formation of a multivalent protein condensate that is dependent on the phosphorylation of the scaffold protein Linker for Activation of T cell (LAT) (Zhang et al., 1998). Following the formation of TCR:pMHC complexes, immune receptor tyrosine-based activation motifs (ITAMs) on the TCR-associated CD3 chains are phosphorylated by the Src family kinase, LCK, creating docking sites for the Syk kinase, ZAP-70 (Chakraborty and Weiss, 2014; Iwashima et al., 1994). ZAP-70 is phosphorylated by LCK and subsequently, ZAP-70 phosphorylates its substrates, which include LAT and SLP-76 (Zhang et al., 1998). The adaptor protein GRB2 has Src-homology 2 (SH2) domains that bind to phosphorylated LAT. GRB2 then binds to the polyproline region (PR)of the guanine nucleotide exchange factor (GEF) son of sevenless (SOS). Since both LAT and SOS-PR are multivalent for GRB2, this leads to crosslinking and condensation of assemblies (Bunnell et al., 2002; Houtman et al., 2006; Huang et al., 2016, 2017; Li et al., 2012; Su et al., 2016). These LAT:Grb2:SOS assemblies propagate MAP kinase and calcium signaling through well-described pathways that culminate in ERK and NFAT translocation (Kortum et al., 2013; Macian, 2005; Podtschaske et al., 2007). In the nucleus, these transcription factors control IL-2 production, T cell differentiation and other effector functions. Thus, LAT assemblies may be considered a hub of proximal TCR signal processing.

LAT assemblies and their constituent molecules have been extensively visualized with up to nanometer precision (Douglass and Vale, 2005; Sherman et al., 2016; Williamson et al., 2011). The colocalization of LAT and other molecules suggests that many molecules associate with these signaling platforms and may dynamically exchange during the lifetime of the assembly (Su et al., 2016). LAT:Grb2:SOS assemblies have also been reconstituted in order to measure the relationship between clustering and the kinetic parameters of associated molecules (Huang et al., 2017). Within LAT assemblies, molecules may experience more limited diffusion, segregation from negative regulatory machinery, and enhanced residency times that promote forward signaling. The

prominent role that LAT assemblies play in T cell signal integration is increasingly appreciated, but the roles of ligand affinity and TCR triggering in causing LAT clustering remain poorly understood.

T cells are capable of activating in response to a small handful of agonists, and can also achieve discrimination within a short period of time (Brodovitch et al., 2015; Delon et al., 1998; Štefanová et al., 2003), emphasizing the high degree of precision required for discrimination of true agonists with subtly different affinities. The failure to sensitively detect agonist ligands or strong responses that occur in response to low affinity pMHCs results in hyperactivation and autoimmunity (Rojas et al., 2018; Wucherpfennig and Strominger, 1995). While an average TCR:pMHC binding dwell time of a few seconds is a feature of some activating pMHC ligands; ligands capable of stimulating at low densities are likely to have dwell times of 10-20 seconds (Stepanek et al., 2014). And recent evidence shows that T cells respond disproportionately to rare, long-dwelling TCR:pMHC binding events (Lin et al., 2019). These long events can be the result of individual dwells of high affinity ligands or may be accumulated as a collection of low affinity, short-lived binding events that are correlated in space and time. Other work has also emphasized the specific sequence and coordination of early T cell signaling events that may allow weak, 'trickle-through' signals to achieve full T cell activation (Germain, 2010; Rosette et al., 2001). Such a mechanism invokes an intracellular memory that records productive ligand encounters. We explore whether LAT phosphorylation and assembly could coordinate binding events and serve as such a memory.

We use primary, transgenic murine T cells (AND TCR) and a recently introduced imaging platform (O'Donoghue et al., 2013) to directly map single molecule TCR:pMHC binding events to LAT assembly and signaling responses within a hybrid live cell-supported membrane junction. We show, for the first time, that single TCR:pMHC complexes trigger the formation of localized LAT condensates. However, bona fide TCR ligation, even from weak ligands that cannot activate T cells, can produce sufficient signals for LAT assembly. Once triggered, LAT assemblies are observed to be self-limiting in the sense that all assemblies show a similar first-order decay process that is uncorrelated with the unbinding of the pMHC. Here, we measure how the T cell integrates both the sequence of individual TCR:pMHC complexes and LAT assemblies in order to reach early cellular activation, as read out by NFAT translocation. Using this assay, we show that the rate of LAT cluster accumulation correlates with T cell activation, regardless of peptide affinity, suggesting that LAT assembly is a key signaling currency in T cells. During the window of data acquisition, the number of LAT clusters exceeds the number of TCR:pMHC ligation events, and is proportional to pMHC affinity. Taken together, we detail the relationship between single TCR triggering, ligand discrimination and signal integration via LAT:Grb2:SOS assemblies during early T cell decision-making.

Single TCR:pMHC binding events trigger LAT assembly

We implemented an approach to visualize individual TCR binding of agonist-peptide-MHC while simultaneously detecting clustering of LAT molecules in the same living T cell at a live cell-supported bilayer interface. This molecular impulse-response assay entails mapping individual binding events to cellular responses. A similar hybrid live cell-supported membrane assay has been implemented to track single molecule TCR:pMHC complexes and measure the recruitment of the kinase ZAP-70, and more recently, to the outcome of the calcium signaling pathway activation based on NFAT translocation (Lin et al., 2019; O'Donoghue et al., 2013; Pielak et al., 2017). We extend this strategy to visualize the assembly of LAT localized to TCR:pMHC binding events. ZAP-70 recruits to phosphorylated TCR, then phosphorylates the membrane-associated scaffold, LAT, which forms extended assemblies through crosslinking via Grb2 and SOS (Balagopalan et al., 2015). LAT assemblies potentiate downstream signaling that culminates in T cell activation. These signaling activities are summarized in **Figure 1a**. T cells normally encounter ligands at low densities and likely can respond to a few tens of agonists. Ten agonist molecules at the APC:TC interface (Delon et al., 1998; Demotz et al., 1990) would yield an agonist density on the order of ≈0.1 pMHC/μm^2. Because of this expected low density of presentation, we seek to capture each individual TCR:pMHC complex directly by fluorescence imaging and map its contribution to cellular activation.

T cells are deposited onto supported lipid bilayers (SLBs) with Ni^{2+}-chelating lipids that display histidine-tagged intercellular adhesion molecule-1 (ICAM-1; at hundreds of molecules μm^{-2}) and histidine-tagged peptide-loaded MHC class II (IE^k) to promote cell adhesion and spreading and TCR triggering, respectively (Nye and Groves, 2008; O'Donoghue et al., 2013). This SLB functions as a minimal mimetic for an antigen presenting cell (APC). Measurements are made using mature, differentiated, peripheral, murine $CD4^+$ T cells, unless otherwise specified, which express the recombinant AND TCR recognizing IE^k-bound peptides. A panel of peptide agonists, based on the strong affinity peptide moth cytochrome C (MCC), was used to trigger TCRs. The peptides were HPLC-purified and bear a single organic fluorophore through a thio-maleimide bond. pMHC ligand densities are carefully controlled over three orders of magnitude (<1 to hundreds molecules μm^{-2}) from sub-activation to supra-activation densities that readily form immunological synapses (Dustin and Baldari, 2017). Cells were differentiated from thymic and splenic tissues from 6-10 week old transgenic mice and retrovirally transduced with fluorescent protein-tagged expression constructs.

Membrane-selective imaging by total internal reflection fluorescence microscopy (TIRF-M) enables the detection of small, discrete single TCR:pMHC binding events at the cell surface (**Figure 1b**). Once contact is established, individual TCRs bound to pMHCs are resolved by virtue of their slowed mobility. In the absence of cells, pMHCs on the bilayer undergo free diffusion and are easily localized with short exposures and high excitation

power (20 ms and 0.2 W/cm^2). Bound pMHC are easily discriminated from free pMHC using long exposures and lower incident powers (500 ms and 0.02 W/cm^2). Under long exposures, free ligand molecules are blurred and bound TCR:pMHC complexes are strongly localized and characterized by single step unbinding (**Figure 1b**) and can be tracked for minutes with minimal photobleaching (Lin et al., 2019; O'Donoghue et al., 2013). The weak agonists T102S and ER60 have mean molecular binding dwell times of 15 and 2 seconds, respectively (Ebert et al., 2009; Pielak et al., 2017; Reay et al., 1994). The measured dwell time distributions are shown in **Figure 1c**. At low densities (≈ 0.2 μm^{-2}), activation probabilities range from less than 10% for ligands of lowest strength to 50% for MCC (Lin et al., 2019). The peptides used cover more than a 20-fold range in potency, based on IL-2 secretion assays (Reay et al., 1994).

For impulse-response measurements, T cells were transduced with LAT-GFP with an average overexpression level of 1.3-fold (Supplmental Analysis – Number of LAT molecules). T cells were pipetted into the imaging chamber and after landing on the supported membrane the cells spread and crawled due to association of leukocyte function associated antigen 1 (LFA-1) ligation with ICAM-1. T cells on the SLB formed an essentially planar interface as assessed by reflection interference contrast microscopy (RICM). Imaging of the pMHC channel, in which we detect binding events, happens sequentially with the imaging of fluorescently tagged LAT. We regularly detect LAT condensation localized to TCR:pMHC binding events (**Figure 1d**). The binding event undergoes single step unbinding, confirming that it is single molecule. LAT clusters are also tracked to measure their duration and spatial coordinates. There is a noticeable lag time in LAT assembly onset after TCR:pMHC complex formation, consistent with kinetic proofreading and the biochemical processes preceding LAT assembly (McKeithan, 1995; Stepanek et al., 2014). The localized LAT cluster grows over approximately 10 seconds before undergoing an approximately first order decay process. For the case of long dwelling MCC peptide, the TCR disengagement from the pMHC often occurs tens of seconds after LAT has fully disassembled (**Figure 1e**), although other kinetic sequences are also observed.

The amplitude and lifetime of LAT assemblies are uncorrelated with the duration of the originating binding event.

Key features of any signal are its amplitude and duration. To measure the signaling potential of LAT assemblies localized to TCR:pMHC we estimated the number of LAT molecules in each assembly and measured the lifetime of the cluster. To quantify the number of LAT molecules we combined information from western blot analysis,

transduction efficiency, and single-molecule LAT-eGFP brightness distributions (Supplemental Analysis – Number of LAT molecules). The estimated total background

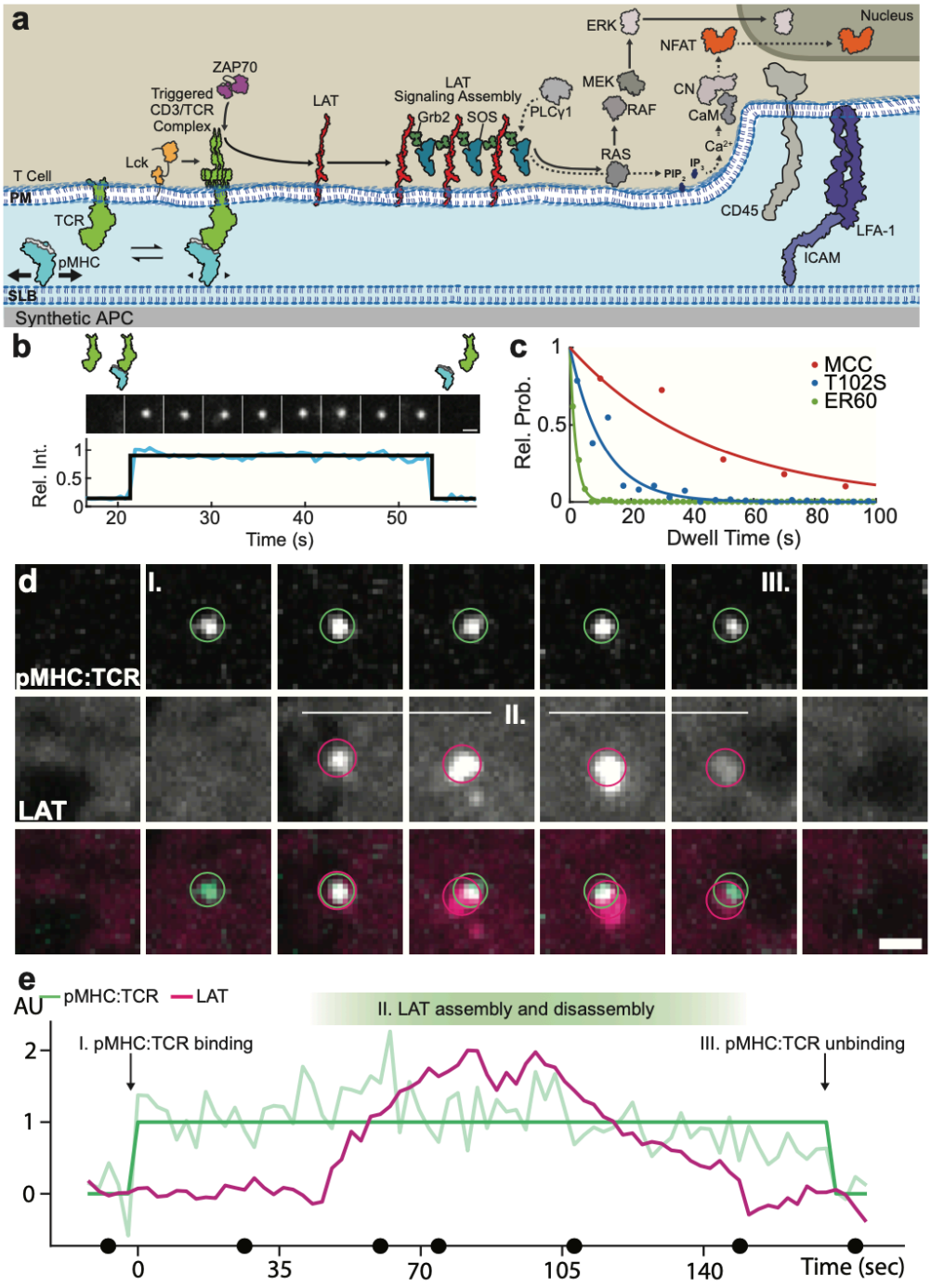

Figure 1-1. Single TCR:pMHC complexes trigger LAT assembly.
(a) Schematic of T cell signaling at a live cell-supported lipid bilayer interface. pMHC displayed on a supported lipid bilayer binds to cell surface TCR and transitions from rapid diffusion (large arrows) to slowed mobility (small arrows). (b) Single TCR:pMHC binding event. A ligand:receptor complex is visualized in TIRF using a long exposure time (500 ms, 0.1W/cm^2). Binding and unbinding occur in single fluorescent intensity steps. (c) Molecular binding dwell time distributions for MCC, T102S and ER60 peptides. Measured single molecule dwell times are shown as scatter points in

blue, red and green, respectively. The population distribution, fit to a single exponential, is shown by the corresponding colored line. Data from more than 300 trajectories from at least 4 single cells differentiated from 2 mice. (d) Montage of a single TCR:pMHC binding event leading to a subsequent, colocalized LAT assembly. Binding event circled in green and LAT assembly in magenta. (e) Intensity quantification of event shown in (d) with black points on time axis indicating the time of frames used in (d).

LAT (endogenous with exogenous) ranged from 1000 μm^{-2} to 2500 μm^{-2}, with exogenous LAT-eGFP being expressed at an average of 1.3 times the endogenous LAT for these experiments. Although LAT was fairly uniform across the membrane, there were still significant heterogeneities. To calculate the number of LAT molecules that accumulated within the assembly, we demarcated background LAT levels from those within the assembly (**Figure 2a**). Utilizing the median background pixel intensity as the local background we found that the mean number of LAT molecules that maximally accumulated within the clusters to be ≈0.33 of the background density (in μm^{-2}) across cellular expression levels (**Figure 2b**). For example, a local background density of 900 μm^{-2} would likely accumulate ≈300 LAT molecules at its maximum size. This estimate is

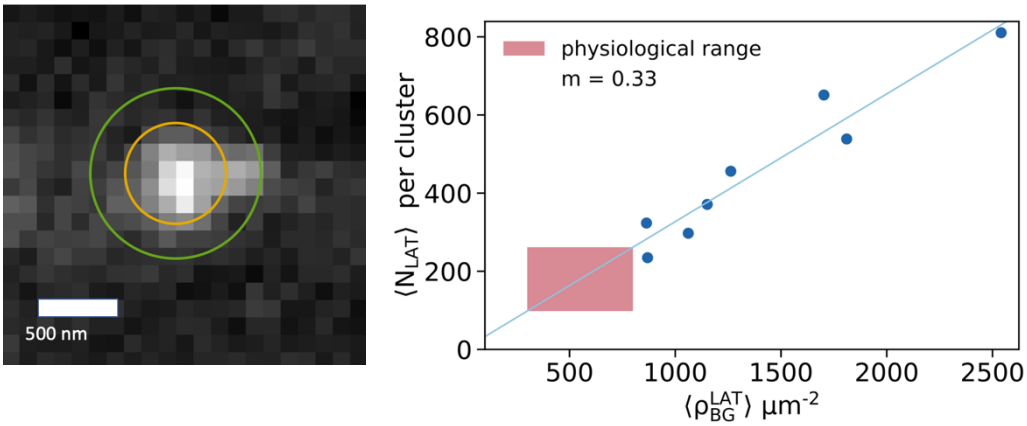

Figure 1-2. Quantification of LAT assemblies.
Left: Background pixels are those between the inner orange ring and the outer green ring.
Right: Scatter plot showing the average number of net LAT within the cluster as a function of the average density of background LAT.

different than the ≈49 molecules estimated by Williamson et al., however they used PALM to measure cluster sizes in cells stimulated with bulk antibody that were then fixed (Williamson et al., 2011), likely creating a significantly different organization of LAT compared to low density pMHC stimulation on live cells. The lifetime of the assemblies was measured as the length in time between the initial detection of the LAT cluster and its final detection. Importantly, we analyzed LAT clusters that assembled locally to a TCR:pMHC binding event.

To detect whether the size or lifetime of LAT clusters encoded any information about the dwell time of the ligand we correlated ligand dwell time with the size and lifetime of the LAT cluster is produced (**Figure 3a** and **b**). The lack of correlation between pMHC binding dwell time and LAT cluster properties suggests that LAT assembly characteristics

are independent of the triggering pMHC dwell time. If T cells are exclusively sensitive to dwell time, then TCR:pMHC dwell time is not being read-out in size or duration of LAT clusters. However, as we will see later, the probability of assembly formation is sensitive to TCR:pMHC dwell time. In many cases LAT assemblies were observed to become spatially separated from binding events over time. This apparent excursion of LAT assemblies could reach distances of ≈400 nanometers (**Figure 3c-d**) and is a potential explanation for the decoupling of LAT characteristics from TCR dwell time with pMHC.

LAT assemblies include active LCK and ZAP-70 molecules

In addition to the size and lifetime of clusters, their composition is important for understanding the mechanism of their formation. LCK and ZAP-70 are known to mediate TCR triggering and LAT phosphorylation, respectively. Multiple LAT tyrosines must be phosphorylated for assembly formation through SOS-mediated scaffolding of Grb2 molecules (Houtman et al., 2006; Kortum et al., 2013). Following ligation, TCR:pMHC complexes are thought to encounter active LCK:CD4 receptor complexes in a process called co-receptor scanning (Stepanek et al., 2014). LCK is a plasma membrane-anchored Src family kinase with a membrane-proximal Src-homology 3 (SH3) and an SH2 domain. Early regulatory mechanisms of T cell signaling have been well-studied (Gaud et al., 2018). Briefly, catalytic activity of LCK is regulated by phosphorylation of an inhibitory tyrosine (Y505) and an activating tyrosine (Y394). Dephosphorylation of tyrosine 505 by CD45 leads to a conformational change that precedes full activation and enzyme opening upon phosphorylation at tyrosine 394. Upon recruitment and activation, LCK phosphorylates TCR ITAM residues, creating docking sites for ZAP-70. ZAP-70 is a Syk family kinase that docks on ITAM motifs via its tandem SH2 domains. Phosphorylation of ZAP-70 at tyrosine 314 by LCK and subsequent autophosphorylation at tyrosine 493 leads to full kinase activation (Au-Yeung et al., 2017).

We probed the localization of endogenous LCK and ZAP-70 in LAT assemblies at low pMHC ligand densities by immunofluorescence. We detected the conformation and residue-specific states of LCK and ZAP-70 in murine T cells expressing LAT-GFP. Clusters of LCK and ZAP-70 molecules are visualized alongside LAT clusters (**Figure 3e-f**). Using LAT assemblies as a mask, we quantified the probability of localizing phosphotyrosine forms of the upstream kinases (Supplemental Analysis – Immunofluorescence). Both LCK and ZAP-70 localize with LAT clusters, but the active forms of each kinase had the highest probabilities of co-localization LAT clusters. Thus, LCK and ZAP-70 are found in LAT clusters, regardless of the presence of TCR:pMHC complexes. This fact will be important for interpreting results in later sections exploring the super-numerosity of LAT relative to the number of binding events.

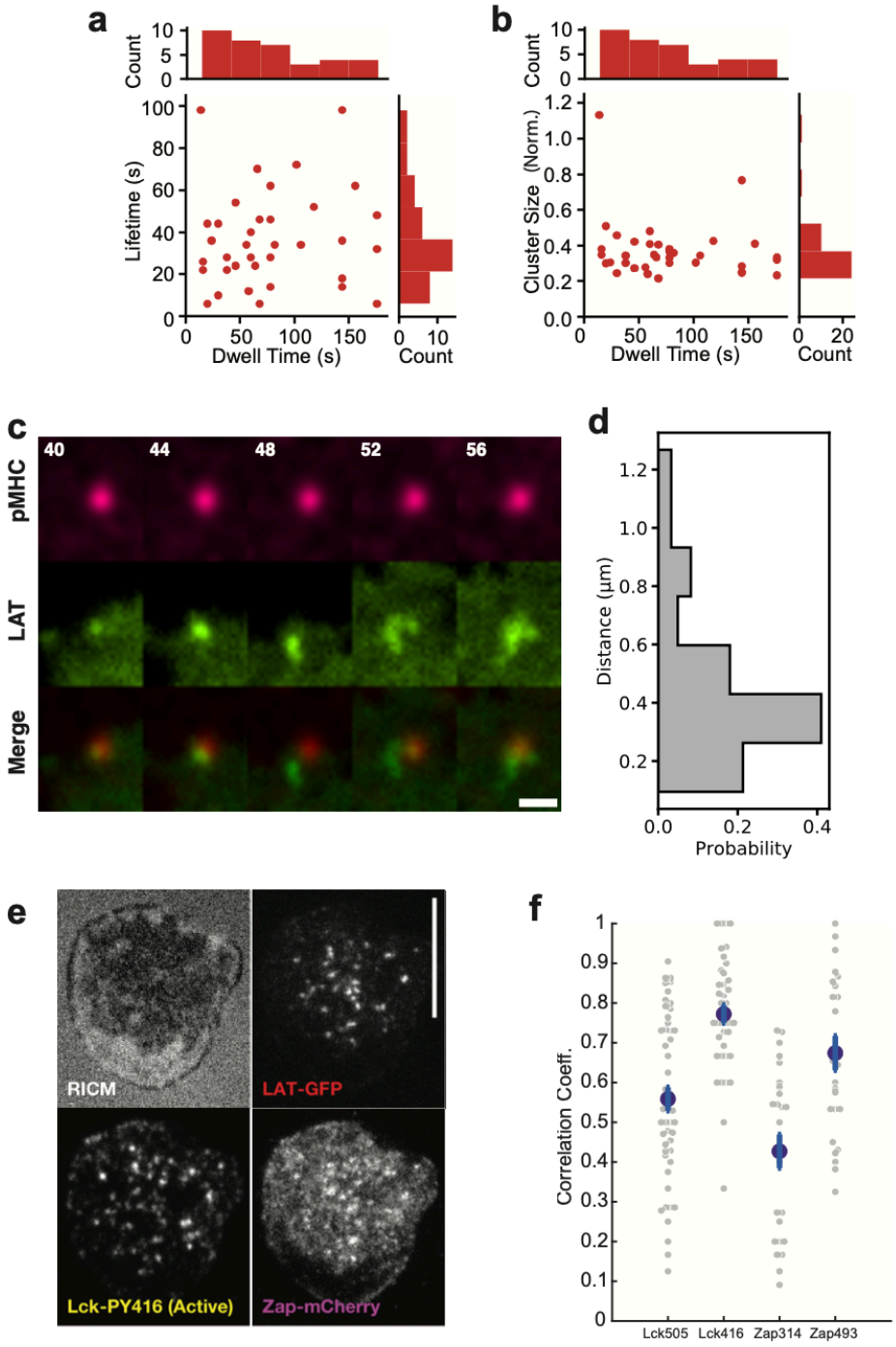

Figure 1-3. Biophysical features of LAT assemblies are discrete.
(a) LAT lifetime versus binding event dwell time for individual LAT assemblies originating from single MCC-MHC:TCR complexes. Each distribution contains >70 LAT cluster intensity traces. (b) Maximal LAT cluster size normalized to background density (μm^{-2}) versus binding event dwell time for individual LAT assemblies originating from single MCC-MHC:TCR complexes. Each distribution contains >70 LAT cluster intensity traces. (c) Montage of a LAT assembly that forms in response to a TCR:pMHC binding event that then undergoes spatial separation from the original, colocalized position. The pMHC channel was gaussian filtered to emphasize localization of pMHC. (d) Distribution of maximum spatial offsets between LAT assemblies and their initiating TCR:pMHC binding events. (e) Immunofluorescent labeling

of LCK pY416 (active form of LCK) in a cell expressing both ZAP-70-mCherry and LAT-GFP. RICM indicates cell-bilayer interface. Scale bar = 5 μm. (f) Distribution of single cell correlation coefficients for specific phosphorylated forms of LCK or ZAP-70 and LAT-GFP clusters (from immunofluorescence images). LCK Y505 detects the inactive form and LCK Y416 detects the active form. ZAP-70 Y314 detects the primed state and ZAP-70 Y493 detects the active state. Each gray point represents a cell. Purple spot indicates population mean and blue bars reflect S.E.M. (N > 30 for each condition).

The probability of LAT assembly formation correlates with TCR:pMHC binding dwell time

The size and lifetime of a LAT cluster does not seem to encode any information about the dwell time of the initiating binding event (**Figure 2a and 2b**). That is, there is no analog response of LAT cluster attributes to dwell time. However, we find that the probability of a binding event to produce a LAT assembly is an increasing function of dwell time. pMHC binding events can be broadly classified as productive if they produce a local LAT assembly, otherwise they are considered unproductive. The ensemble of dwell times is roughly exponential (**Figure 4a** and **4b**). By partitioning this dwell time distribution into productive and unproductive dwell events we can consider the relative probability that a binding event is productive over the probability of it being unproductive (**Figure 4c**) we find that both MCC and T102S produce similar dwell time response curves. This suggests that the stimulatory capacity of any pMHC is encoded entirely by its dwell time. The reason high-affinity peptides are potent stimulators of TCR is due to the increased abundance of long dwelling events that productively signal to LAT.

LAT clusters may form from non-TCR pathways (Balagopalan et al., 2018; Raab et al., 2017). Therefore, to understand how *total* LAT cluster formation depends upon TCR stimulation we made bilayers with matched densities of a variety of peptides and measured the extent of LAT clustering as a function of peptide identity. Murine AND T cells were exposed to bilayers displaying ICAM-1 and null peptide, T102E (hundreds/μm^2) to recapitulate the abundant, non-stimulatory ligands encountered in typical presentation. Time series data were collected to construct the number of LAT assemblies produced over time (**Figure 5a**). During the first 3 minutes of interactions with surfaces bearing only adhesion or null ligands, single T cells generated 1-10 LAT clusters (**Figure 5a**, rows 1-2). From this low basal state, LAT clustering increased proportionally with peptide strength (**Figure 5a**, rows 3-5). The rate of LAT clustering during early signaling increased 7-fold for T102S and 15-fold for MCC. Within the limits of our temporal resolution, the very weak agonist ER60 was indistinguishable from adhesion-only or non-agonist conditions.

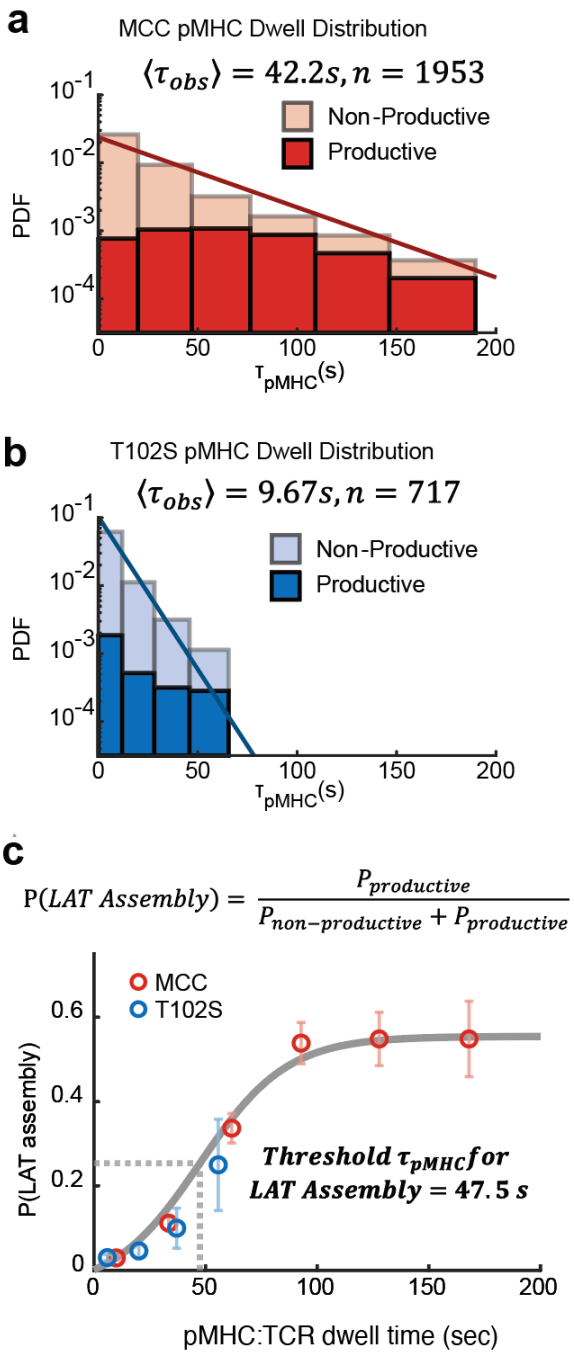

Figure 1-4. Probability of a binding event to produce a LAT assembly.
a) MCC-MHC:TCR dwell time distribution. Light colored probability distribution function (PDF) is of unproductive binding events, it follows an exponential distribution. The dark colored PDF is of productive binding events. b) T102S-MHC:TCR dwell time distribution. Light colored probability distribution function (PDF) is of unproductive binding events, it follows an exponential distribution. The dark colored PDF is of productive binding events.
c) Relative probability of producing a LAT assembly. The ratio of the "productive" to "unproductive" points in the bins in (a) and (b) form a sigmoidal response curve to dwell time.

By comparison to the murine AND T cells, the most common model human T cell line, Jurkat leukemia cells, readily formed LAT assemblies on human ICAM-1-only bilayers (**Figure 5b**, row 1). Differentiated, primary human $CD4^+$ T cells behaved like the AND T cells and experienced minimal LAT clustering in the absence of TCR clustering (**Figure 5b**, row 3). In both cases of human T cells, TCR triggering by bilavent antibody on the bilayer resulted in an approximately 4-fold increase in LAT clustering (**Figure 5b**, rows 2 and 4). Taken together, these observations argue that primary T cells are tuned to sensitively signal through LAT assemblies in response to TCR triggering. However, we were still able to observe the formation TCR localized LAT clusters (Supplemental Analysis – LAT clusters in Jurkats).

The number of LAT clusters exceeds the number of TCR:pMHC complexes

By measuring both the number of binding events and the number of LAT clusters from initiation of contact and signaling, we observed that LAT signaling assemblies could be more numerous than bound receptors (**Figure 6a-b**). Since the dwell time distribution is well-described by a single exponential, we estimated the number of binding events that are missed due to their brief durations or photobleaching (see Supplemental Analysis – Calculating Missed Binding Events). We quantified the ratio of total number of LAT clusters over the total number of pMHC binding events during the first 3.5 minutes of T cell interactions with the substrate. The ratio is highest for MCC peptides with a mean value greater than 2. The ratio decreases for the weaker T102S agonist to 1 and is much less than 1 for ER60 (**Figure 6b**). We note that a ratio of 1 does not suggest that each binding event produces a LAT assembly. Rather, the data suggest that the rare long dwelling events are capable stimulating multiple LAT clusters, likely through a variety of cross-talk pathways.

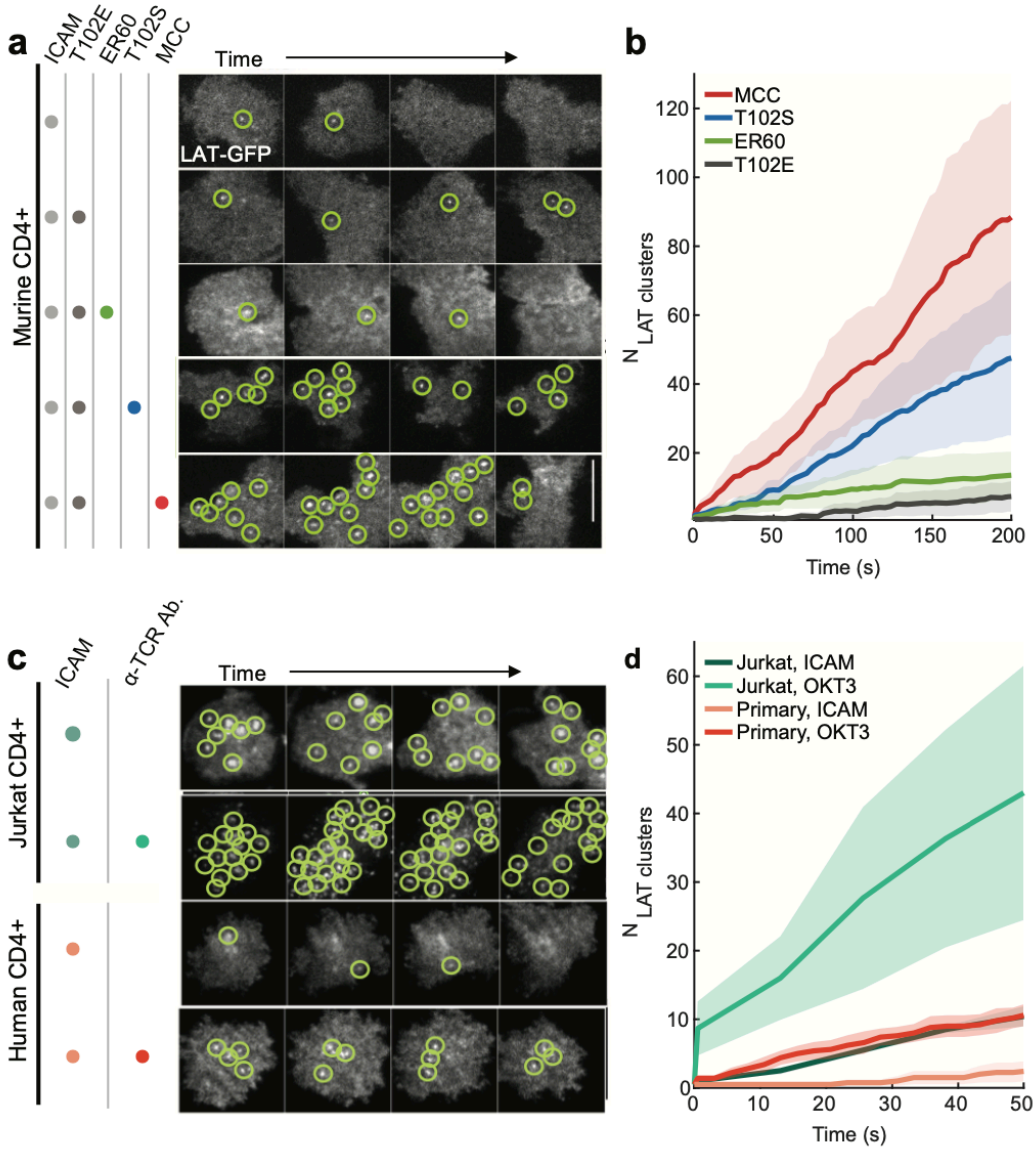

Figure 1-5. T cells accumulate LAT clusters in response to bona fide TCR triggering.
(a) Single cell LAT-eGFP time series for AND T cells exposed to adhesion (ICAM), T102E-MHC (self-peptide), and agonist pMHCs (ER60 < T102S < MCC in potency). Each row represents a condition whose ligand composition is indicated by the table on the left. ICAM and T102E are present at high densities (~200 um^{-2}), and agonist peptides are all at 0.2 um^{-2}. LAT clusters circled in green. (b) Traces of mean single cell LAT cluster accumulation (standard deviation is shown as corresponding shaded area). N > 4 for each condition. Scale bar = 5 µm.
(c) Single cell LAT-GFP time series for human T cells (Jurkat cell line or primary human CD4+ T cells) exposed to adhesion (ICAM), and anti-TCR antibodies (OKT3). Each row represents a condition whose ligand composition is indicated by the table on the left. ICAM is present at ~200 um^{-2} and OKT3 is at 0.2 um^{-2}. LAT clusters circled in green. (d) Traces of mean single cell LAT cluster accumulation (standard deviation is shown as corresponding shaded area). N > 4 for each condition. Scale bar = 5 µm.

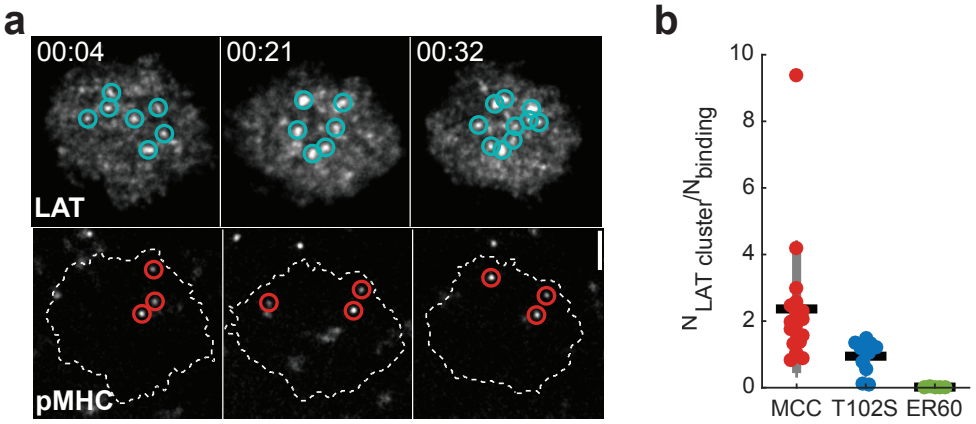

Figure 1-6. LAT assemblies outnumber TCR:pMHC complexes as a function of affinity.
(a) Example single cell LAT-eGFP (top) and fluorescent pMHC (bottom) time series showing that the number of LAT clusters (cyan) accumulated is greater than the number of TCR:pMHC binding events (red). Cell outline in white, dash line. Scale bar = 3 μm. (b) Distribution of the ratio of the number of LAT clusters over the number of TCR:pMHC binding events for cells exposed to different peptides at 0.2 μm^{-2}. Each point represents a single cell, and black and gray bars indicate the population mean and standard deviation, respectively.

T cell activation correlates with the number of LAT assemblies

Given the finding that the number of LAT assemblies was a function of the peptide ligand strength, we explored the relationship between discrete LAT clusters and cellular decision-making. We applied the molecular impulse-response assay to map individual TCR binding events to intermediate (LAT assembly) and downstream (NFAT translocation) outcomes (**Figure 7a**). We took advantage of cloning based on the P2A self-cleavable peptide system (Liu et al., 2017) in order to transduce T cells with an NFAT-mCherry-P2A-LAT-eGFP bicistronic construct. The tandem construct leads to efficient expression of LAT and NFAT in the same cell (**Figure 7a-b**). Most other approaches compare cellular behaviors across an ensemble of genetically identical, yet copy number variant cells, here we capture single cell heterogeneity throughout the signal integration process.

To monitor NFAT translocation, cells are imaged using epifluorescent illumination from a mercury arc lamp. A series of images from three to six microns above the SLB enables finding the optimal plane to determine NFAT translocation. A typical imaging sequence includes RICM images to detect cell-bilayer contact and interfacial area, TIRF images of both TCR:pMHC and LAT clusters at a frequency of ≈4 seconds, and NFAT images at a lower frequency, typically 30 seconds (**Figure 7b**). Initial NFAT translocation typically

occurs before 8 minutes. The first observation of NFAT nuclear localization, measured as an inversion in the ratio of nuclear to cytoplasmic signal is designated as the activation timepoint (Lin et al., 2019).

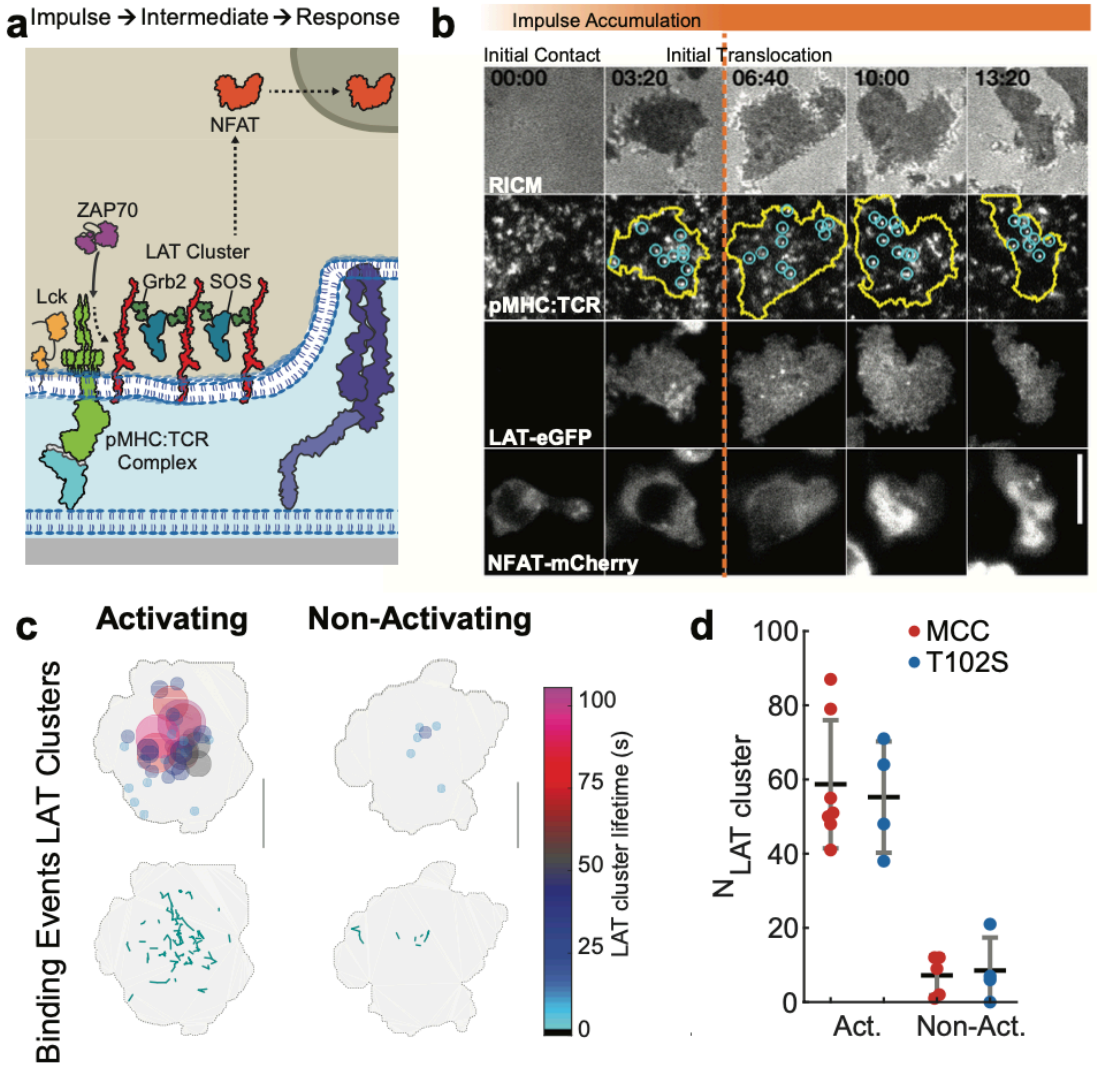

Figure 1-7. LAT assembly accumulation rate correlates with early T cell activation.
(a) Schematic of the impulse-intermediate-response assay. TCR:pMHC binding events are the inputs, LAT clusters are the intermediates, and NFAT nuclear translocation is the early activation response. (b) Example data for an activating T cell. RICM (top), fluorescent pMHC (second row), LAT-FP (third row), and NFAT-FP (bottom) time series show a T cell landing, spreading, accumulating TCR:pMHC binding events (Impulse) and LAT clusters (Intermediate), and translocating NFAT (Response). Bound pMHC are resolved using long (500 milliseconds) exposure times (bound pMHC molecules are circled in cyan, cell outline shown as yellow lines). Activation time is defined as the first observation of NFAT translocation (indicated by orange, dotted line). Scale bar = 3 μm. (c) Spatial maps of TCR:pMHC trajectories (top) for an activating and a non-activating cell exposed to MCC-MHC. LAT cluster earthquake maps (bottom) for corresponding cells; size and color of each spot indicate the duration of the LAT assembly. (d) Distribution of the number of LAT assemblies for activating and non-activating cells exposed to distinct pMHCs at the same density (0.2 μm^{-2}, counted for up to 200 seconds). Each point in the scatter plot is of a single cell.

The signaling inputs and LAT assemblies accumulated by representative single cells is shown in **Figure 7c**. The footprint of the cell is plotted based on RICM detection of T cell contact with the SLB. The spatial and temporal features of binding events and LAT assemblies show greater numbers of each for activating cells. LAT cluster lifetimes are also longer in activating cells (**Figure 7c**). The number of LAT assemblies is extracted for 4-7 cells measured for each of the T102S and MCC agonist peptides, at the same, low ligand density (0.2 pMHC/μm^2). Strikingly, the number of LAT assemblies accumulated is much higher in activating cells and very similar for low and high affinity ligands (**Figure 7d**). This suggests that the number of LAT assemblies strongly correlates with the activation of single T cells.

LAT:Grb2:SOS protein condensation phase transition may integrate correlated TCR:pMHC binding events

It has been shown that spatially close and temporally coincident binding events may cooperate to propagate downstream signal (Lin et al., 2019; Manz et al., 2011). To investigate whether LAT may function as the integrator of disparate binding events we imaged AND T cells expressing Zap-mCherry-P2A-LAT-GFP. In the case of MCC:MHC, whose mean dwell time is almost 50 seconds, individual long-dwelling binding events readily result in substantial ZAP-70 accumulation at the membrane and LAT assembly (**Figure 8a**). A single T102S:MHC binding event, whose mean duration is less than 10 seconds, has a lower probability of generating a LAT assembly (**Figure 4b** and **6b**). Filtering T102S trajectories on cells that would eventually activate, we regularly found binding trajectories that occur within 2 microns and 30 seconds of each other. Moreover, these cooperative binding events correlated with abundant ZAP-70 recruitment and LAT assembly over the lifetime of those events (**Figure 8b**). These data suggest the coordination between a series of molecules that can satisfy the threshold for signal propagation. Therefore, the machinery of early T cell signaling can respond to rare long dwelling events in isolation as well as a few medium dwelling events that occur within a close proximity. In this way we see that increased concentration of ligand does not enhance signaling merely through occupancy of TCR, but rather in the synergistic effect of being able to collectively push a local region of the T cell passed the threshold for LAT assembly formation.

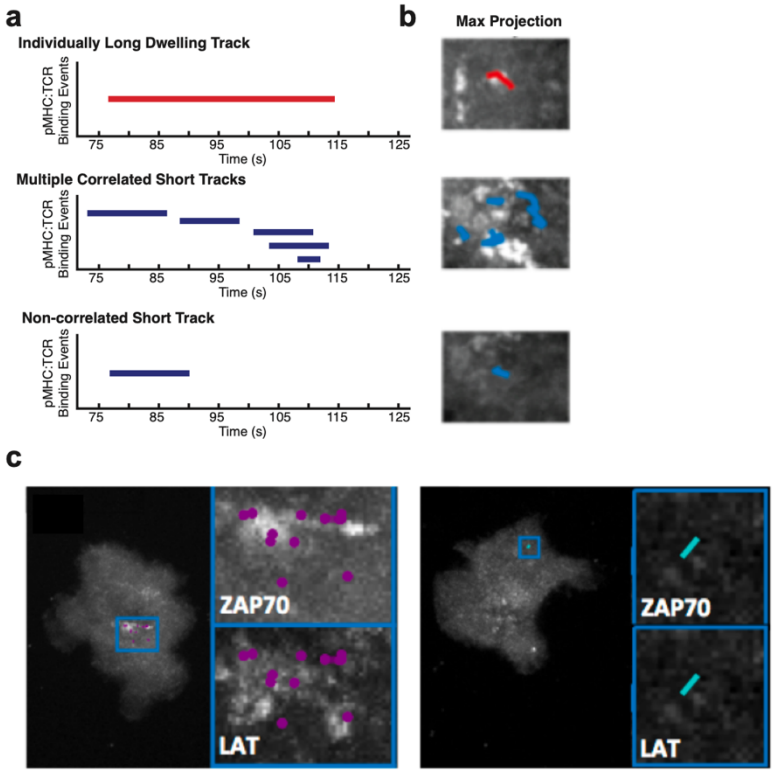

Figure 1-8. Spatiotemporally coordinated binding events increase membrane-associated active ZAP-70. (a) (Top row) A single long-dwelling MCC-MHC:TCR binding event leads to a localized LAT assembly. (Middle row) Multiple spatiotemporally-coupled T102S-MHC:TCR binding events lead to localized LAT assemblies at the membrane. (Bottom row) An isolated, short T102S-MHC:TCR binding event does not generate a LAT assembly. (b) Examples of binding event trajectories described in (a) drawn over a maximum projection of LAT-eGFP throughout the time period of the binding events. (c) Left: Maximum projection of a region of ZAP-70-mCherry and LAT-eGFP accumulation over the duration of a spatiotemporally-correlated series of T102S-MHC:TCR binding events. Right: Maximum projection of a region of ZAP-70-mCherry and LAT-eGFP accumulation over for a singleT102S-MHC:TCR binding event showing no significant signal.

Discussion

T cells are capable of activating following the accumulation of a few agonist binding events whose binding kinetics differ subtly from more abundant self-peptides (Matsui et al., 1994; Tischer and Weiner, 2019). Furthermore, T cells face the challenge of sparsely sampling the dwell time distribution of agonist pMHC, and yet they respond with exquisite accuracy. Using our impulse-response assay, we show that at low densities of agonist-pMHC, single cells achieve activation thresholds through signal amplification via discrete LAT assemblies. Importantly, we measure the distribution of TCR activation as a function of pMHC dwell time. This dwell time response curve is the basic input-response

function which subsequent layers of T cell signaling are built upon. Our study suggests that at low levels of stimulation, LAT clusters act as a discrete signaling currency, and that once a certain number (≈40) are achieved within a small window of time (≈2 minutes) that NFAT will successfully translocate. Moreover, these LAT clusters contain active LCK and ZAP-70 machinery that lie in the upstream signaling cascade. This is consistent with the recently found bridging interaction between LCK and ZAP (Lo et al., 2018). The numbers of LAT assemblies are proportional to the agonist ligand mean dwell time. Thus, ligand discrimination is achieved through the dependence of ZAP-70 activation upon ligand dwell time. And whether this level of activation is sufficient for LAT assembly represents a second layer of kinetic proofreading in T cell signaling.

In this study we have focused primarily on LAT assemblies localized to TCR:pMHC binding events. However, we note that even though these assemblies initiate near the bound TCR (< 100 nm), they typically end up centered ≈400 nm away from the initiating TCR as the cluster is achieves its maximal size. This spatial decoupling is interesting. We observe active LCK and ZAP-70 clusters within all LAT assemblies and that LAT phosphorylation and clustering primarily occurs in response to TCR triggering. Previous studies have shown ZAP-70 release from phosphorylated ITAMs and diffusion within the plane of the plasma membrane (Bunnell et al., 2002; Katz et al., 2016). Here, we show a consequence for ZAP-70 dispersion in the potential formation of remote assemblies, though it is possible some assemblies originate from positive feedback from other pathways (Balagopalan et al., 2018; Raab et al., 2017). We observed that ZAP-70 docks at the membrane in the absence of agonist presence. Thus, full activation and maintenance of active ZAP-70 is tightly regulated. Exactly how active LCK and ZAP concentrate within LAT clusters is unclear. Moreover, given that only one TCR is bound locally, then the clusters of active LCK and ZAP-70 represents some small level signal amplification prior to LAT assembly.

The evidence in this study suggests that short dwelling TCR:pMHC complexes may contribute some ZAP-70 recruitment and activation that is pooled across numerous events. Such a mechanism promotes the LAT clustering necessary for cellular activation without explicit dependence upon individually long TCR:pMHC complexes. Moreover, we measure the dwell-time response curve for MCC and T102S to find them identical, suggesting dwell-time is the fundamental input for TCR triggering. We further show that activating cells accumulate a larger number of LAT assemblies. In conclusion, we find that single or spatiotemporally coupled TCR:pMHC binding events can produce localized LAT assemblies whose size and lifetime are independent of ligand dwell time, which emphasizes the discreteness of the LAT assembly and the role of phase separation in gating the propagation of downstream signaling.

Supplemental Analysis – Calculating Missed Binding Events

To estimate the number of missed binding events we first need a model of the rate of pMHC binding to TCR. If we measure the average rate of binding in the first 40 seconds of the acquisition, when photobleaching is not prevalent, we get a rate of 0.275 binding events per second. Assuming this is a Poisson process we can construct a model of binding (red dots in Figure 9). Next, we divide the first 120 seconds into 8 second bins and count the number of binding events that occur in each bin. Next, we histogram these counts. Here we see that the data fit the Poisson hitting time model quite well.

$$k_{on}^{emp} \approx \frac{n_{obs}}{t} = \frac{11}{40} = 0.275$$

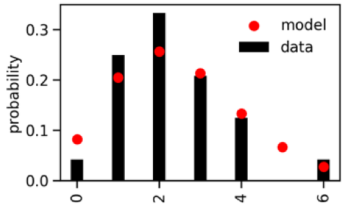

Figure 1-9. Binding events are Poisson distributed in time.

There are two classes of LAT clusters, those we observe to have been born of TCR:pMHC binding, and those without any apparent TCR:pMHC binding, which may arie from photobleached pMHC. Another source of missed binding events are those that bind and unbind in between camera exposures (time-lapse = 2-4 second window). The expected number of total missed binding events is the product of the binding rate with the photobleach curve, augmented by missed short binding events

$$N_{dark\ bind}(t) = k_{on}^{emp} t(1 - e^{-k_{bleach}\, t})/e^{-k_{off}\, t_{time-lapse}}$$

Below we can see that some cells seem to produce LAT clusters only in response to TCR, while in other cases they can originate from other sources. The 95% envelope around the dark-bind curve estimates the variance of the Poisson counting process, and is achieved using a continuous analog of the Poisson distribution (Ilienko, 2013)

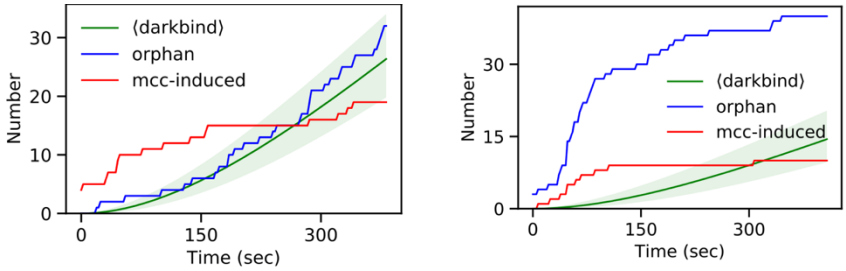

Figure 1-10. Orphan binding as a function of time.

Supplemental Analysis – Number of LAT molecules

In order to estimate the total number of LAT molecules we performed a western blot of the cells that we transduced. See Materials and Methods for transduction of T cells with MSCV-LAT-eGFP. A subset of the batch of cells used in imaging were lysed in 1% Brij lysis buffer. Cell Signal Technology (#9166 – Rabbit anti-LAT) and Santa Cruz Biotechnology (sc-390394 – Mouse anti-GFP) were used for detection. LICOR IRDye 800CW Goat anti-Rabbit and IRDye 680RD Donkey anti-Mouse were used for secondary detection. Given that 14.8 % of the cells were successfully transduced (as assessed by FACS) then ratiometric analysis indicates that LAT-eGFP was expressed at 1.3x the rate of normal WT LAT.

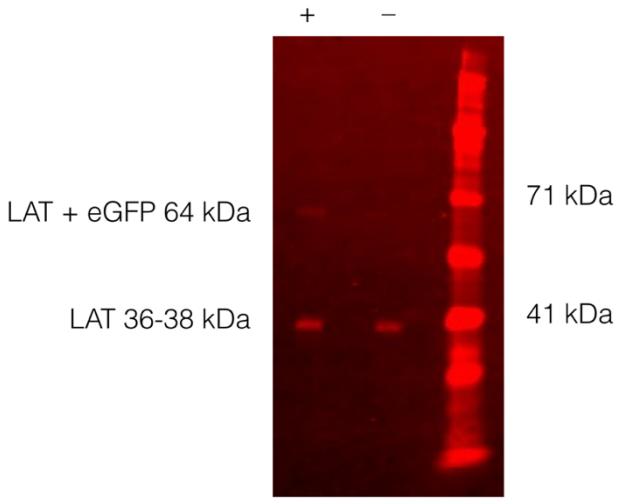

Figure 1-11. Western blot for ratiometric analysis of LAT-eGFP and LAT

Next, we found cells that were low expressors of LAT-eGFP and imaged them to acquire an intensity distribution for single-molecule LAT-eGFP point spread functions. This was scaled by the product of the gain, exposure, and power (GEP) in order to find the linear scaling factor β. This also requires verification that intensity varies linearly with each of gain, exposure, and power. In the equations below D is the "dark" background and I_{net} refers to the net integrated intensity of a single point-spread function.

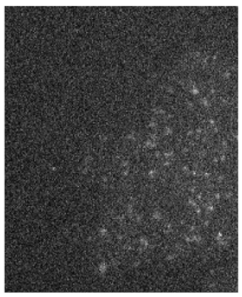

$$T = N_{fl} + N_{endo}$$

$$T = N_{fl}(1 + \alpha)$$

$\alpha \equiv$ ratio of endo over exo

$$\beta N_{fl} GEP + D = I$$

$$\beta = \frac{I_{net}}{GEP}$$

Figure 1-12. Low expression single-molecule LAT-eGFP.

Given that there were hundreds of molecules present we opted for a simple mean estimation of the number of LAT molecules present. Had the intensities suggested a range of tens of molecules then a more sophisticated approach would have been more accurate (Mutch et al., 2007).

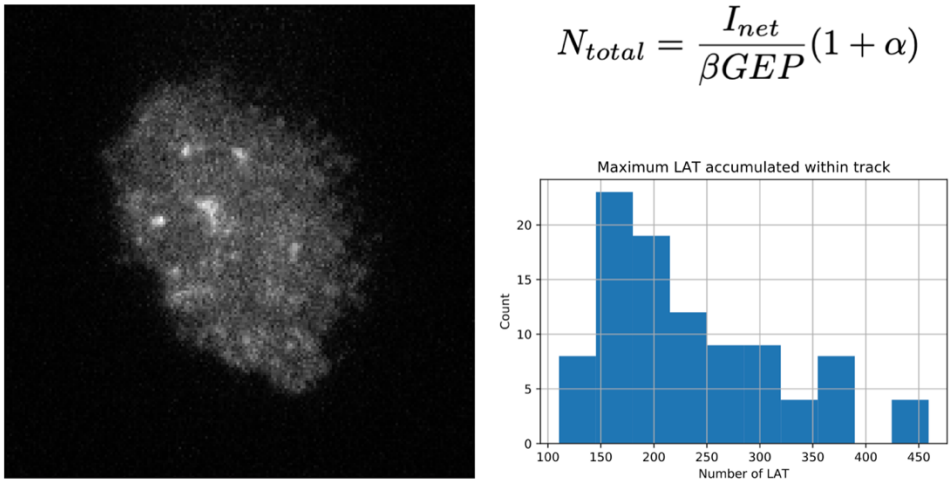

Figure 1-13. Estimation of maximal number of total LAT formed in clusters.

Supplemental Analysis – LAT clusters in Jurkats

In the image below, the left column is fluorescently labeled ligand, the middle column is LAT-eGFP, and the right is an overlay. The top row is of a Jurkat cell on an ICAM only bilayer. The bottom row is of a Jurkat cell on a bilayer with fluorescently labeled anti-human TCR antibody. One can see that on ICAM only there are abundant LAT clusters in Jurkats. On stimulatory bilayers some LAT clusters form localized to antibody, while others have no such correspondence.

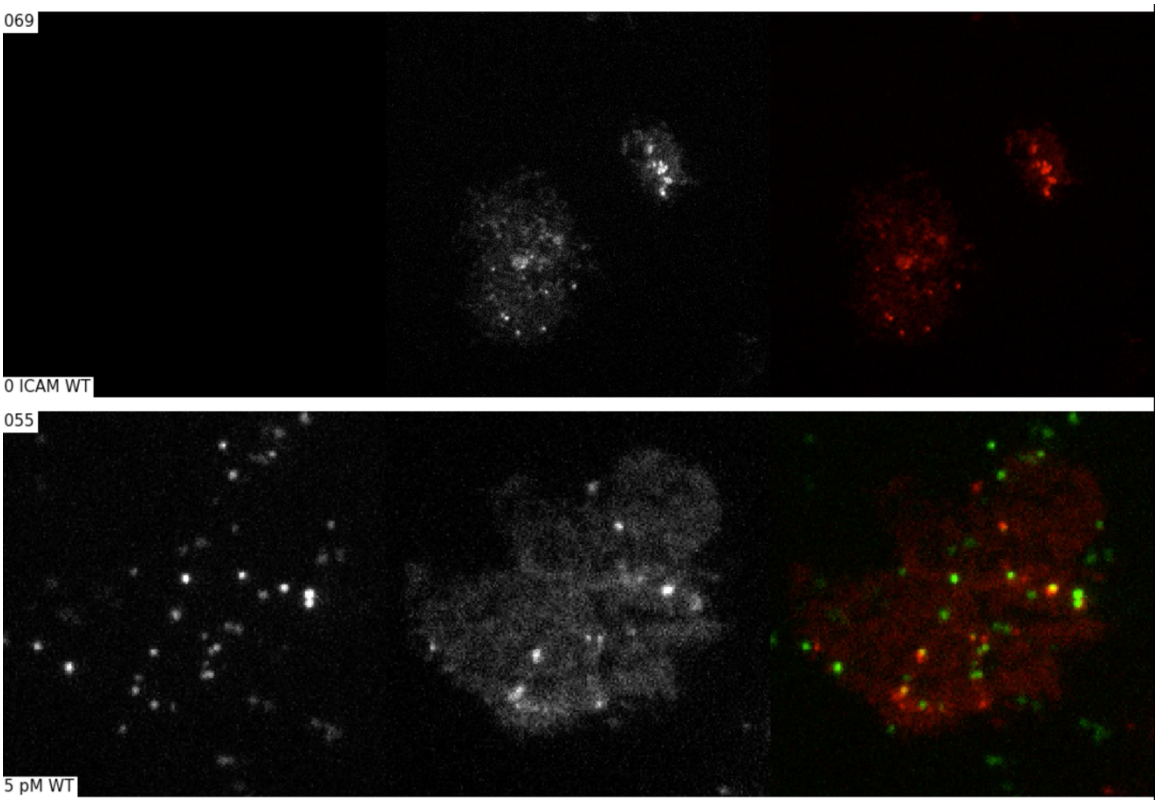

Figure 1-14. Jurkat T cells exhibit basal non-TCR induced LAT clusters.
Jurkat T cells expressing LAT-eGFP were deposited onto adhesion only (top) or stimulatory (bottom) surfaces.
(Top) Jurkat T cell on an ICAM only bilayer.
(Bottom) Jurkat T cell on a bilayer with ICAM and Atto647-labeled anti-human TCR antibody.

Supplemental Analysis – Immunofluorescence

Here we used Mander's Colocalization Coefficient (Dunn et al., 2011) to estimate both the fraction of molecules in LAT clusters as well as the fraction of LAT clusters with molecules of interest. Below is an example for examining pY505. In the bottom row we've masked the LAT channel for those areas that have significant LAT clustering (based upon a brightness threshold) and it is clear that these clusters also contain significant LCK clusters, albeit with the deactivated form (pY505).

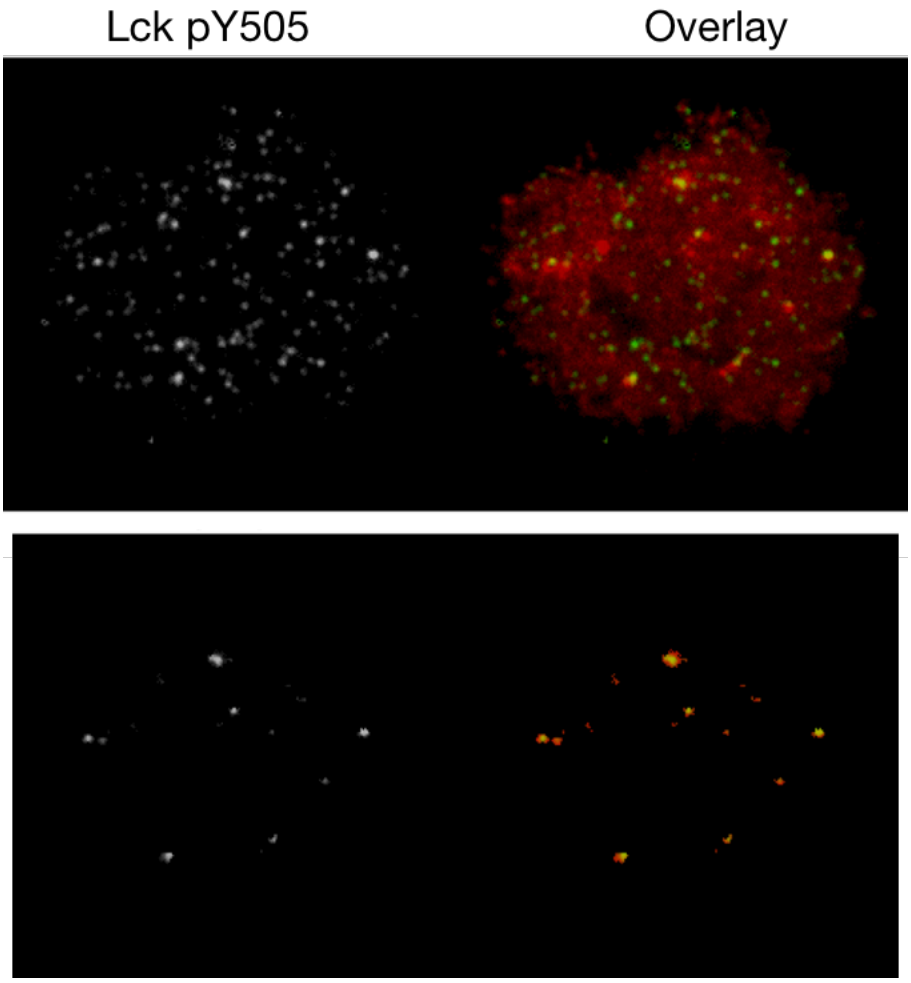

Figure 1-15. Example of Mander's Colocalization Coefficient.
(Top) Left: 647 labeled anti-LCKpY505 Ab. Right: overlay with LAT-eGFP (red).
(Bottom) Using a maximum entropy threshold to select for LAT clusters and masking onto the LCK channel.

Materials and Methods

Bilayer Preparation

Supported lipid bilayers (SLBs) were deposited on piranha-etched, 25 mm, No. 1.5 coverglass in imaging chambers and functionalized with proteins as previously described (O'Donoghue et al., 2013). Briefly, lipid films were prepared with a composition of 98 mol percent 1,2-dioleoyl-sn-glycero-3-phosphocholine (DOPC) and 2 mol percent 1,2 dioleoyl-sn-glycero-3-[(N-(5-amino-1-carboxypentyl) iminodiacetic acid) succinyl] (nickel salt) (Ni2+-NTA-DOGS) (Avanti Polar Lipids, Alabaster, AL). Following resuspension in water, small unilamellar vesicles (SUVs) were formed by tip sonication. Coverslips were sonicated in 1:1 isoporopyl:H_2O and etched for 5 minutes in piranha solution (3:1 H_2SO_4:H_2O_2). Etched coverslips were mounted in Attofluor Cell Chambers (Thermo Fisher, Waltham, MA). SUVs in 2x TBS (TBS; 20 mM Tris, 136 mM NaCl, pH 7.4; Mediatech Inc., Herndon, VA) were deposited onto the glass and SLBs were allowed to form via vesicle rupture for 30 minutes at room temperature. Excess SUVs were removed by washing with TBS and bilayers were activated with 100 mM $NiCl_2$ for 5 minutes. Bilayers were exchanged to live cell imaging buffer (LCB; 1 mM $CaCl_2$, 2 mM $MgCl_2$, 20 mM HEPES, 137 mM NaCl, 5 mM KCl, 0.7 mM Na_2HPO_4, 6 mM d-glucose, and 1% wt/vol bovine serum albumin) and derivatized with pMHC and ICAM-1 at appropriate concentrations (~100 nM) for 35 minutes. Prior to imaging, bilayers were allowed to equilibrate for 35 minutes at 37^{o}C. Cells were suspended in LCB and exposed to bilayers on the microscope. All imaging was performed at 37^{o}C.

Prior to imaging experiments, peptides were loaded overnight on his-MHC II I-E^K (see below for purification) at 37^{o}C in peptide loading buffer (1% wt/vol BSA in PBS, pH 4.5 with citric acid). Prior to loading on bilayers, dye-peptide-MHC complexes were purified over 10,000 MWCO spin concentrators and exchanged to live cell imaging buffer (Vivaspin 500, GE Health Care, Pittsburgh, PA). For Jurkat cells, biotinylated OKT3 Fab fragments were conjugated to 98% DOPC, 0.1% 18:1 Biotinyl Cap PE, 1.9% Ni-DOGS bilayers via streptavidin.

Peptide Purification and Labelling

Three different peptides were displayed on MHC II molecules to cover a range in affinities. All peptides are based on the Moth cytochrome C 88-103 peptide ($MCC_{88\text{-}103}$; MCC) and have been characterized elsewhere (Corse et al., 2010; Huppa, et al., 2010). MCC (ANERADLIAYLKQATK), MCC(C) (ANERADLIAYLKQATKGGSC), T102S (ANERADLIAYLKQASK), T102S(C) (ANERADLIAYLKQASKGGSC) and ER60(C) (GFPTIYFSPANKKLGGSC) were synthesized (David King, HHMI Mass Spectrometry

Laboratory Lab; UC Berkeley) or purchased (Elim Biopharmaceuticals, Hayward, CA). The cysteine-terminal variants bore a short linker and terminated in a cysteine residue for fluorescent labeling with maleimide chemistry.

Dye conjugation of the terminal cysteine peptides was accomplished using a reaction with a maleimide Atto647N fluorophore (Atto-Tec GmbH, Siegen, Germany; described in O'Donoghue, et al., 2013). Fluorescent conjugates were purified using a H_2O:acetonitrile gradient on a C_{18} reverse phase column (Grace Vydae, Deerfield, IL) on the AKTA Explorer 100 FPLC system (Amersham Pharmacia Biotech, Piscataway,NJ). Following labeling and purification, all peptides were confirmed by mass spectrometry.

Protein Purification and Labelling

For display on nickel-chelating lipids, histidine-tagged versions of major histocompatibility complex (MHC) class II I-E^K and murine ICAM-I were purified from bacmid-infected insect cells as described previously (Nye and Groves, 2008). Briefly, a MHC II-hexahistidine construct was expressed in SF9 cells and purified on a Ni-NTA-agarose affinity column (Qiagen). ICAM-I-decahistidine was similarly purified from High Five cells (Thermo Fisher Scientific, Waltham, MA). The MHC and ICAM bacmids were gifts from Dr. Mark Davis (Stanford).

Details of the human ICAM purification can be found elsewhere (Alfieri, 2015). Briefly, a protein construct containing the extracellular domain of human ICAM-1 (residues 28-453) fused to a C-terminal decahistidine tag (ICAM-1-His10) was cloned into a pFastbac1 vector and introduced into the bac-to-bac insect cell/baculovirus based expression system. The protein was secreted from infected High5 cells and captured on Ni - nitrilotriacetic acid (NTA) agarose resin and subsequently eluted. This protein was then titrated on 2% Ni-DGS bilayers testing for cellular adhesion to find optimal concentration of active ICAM-1.

DNA Constructs

T cells were transduced with constructs based on either pMSCV (murine cells) or pHRSIN (human cells) backbones. A GFP-tagged version of LAT was generated in each backbone and served as the template for further cloning. The NFAT1 construct was described previously (Lin et al., 2019) and an mCherry version was used in the construction of the MSCV-LAT-eGFP-P2A-NFAT-mCherry. For ZAP-70 the construct was described previously (O'Donoghue et al., 2013) and an mCherry version was used in the construction of MSCV-ZAP-70-mCherry-P2A-LAT-eGFP.

T Cell Preparation

CD4+ T cells were differentiated from lymph nodes and spleens isolated from AND x B10.BR transgenic mice (Jackson Laboratory) between 6-16 weeks of age following previously established protocols (O'Donoghue et al., 2013; Yu et al., 2010). All animal work was performed with prior approval by Lawrence Berkeley National Laboratory Animal Welfare and Research Committee (AWRC) under the approved protocol 17703.

T cells were cultured in RVC media (DMEM supplemented with 10% FBS, 1x NEAA, 1x Arg/Asn/Folic Acid mix, 1x MEM, 1x NaPyr, 1x Pen/Strep, 1x L-glut, 50 μM βME). Each of the 1x reagents is available as a 100x concentration from Fisher-Scientific. T cells were retrovirally transduced using Platinum-Eco cell-derived supernatants. Platinum-Eco cells (CellBioLabs, San Diego, CA) were transfected with the desired plasmid using linear, polycationic PEI (Sigma-Aldrich) or Lipofectamine 2000 (Thermo Fisher Scientific, Waltham, MA), and retrovirus was secreted into RVC medium at 32^{o}C for 24-48 hours. After resuspending the day 3 cells in the viral supernatant with polybrene they were centrifuged at 1500 rcf for 1 hour to facilitate transduction. They then recovered at 37^{o}C for at least 1 day. Bilayers were contained in Attofluor chambers and 0.2 - 1 million cells were added to each bilayer. Jurkat T cells were maintained in RPMI supplemented with 10% heat-inactivated fetal bovine serum.

Antibodies and Immunofluorescence

At specified timepoints, primary cells were fixed with 2%, ice-cold PFA (VWR, Radnor, PA) for 10-20 seconds. Following rinses with 1x PBS, fixed samples were permeabilized with 0.1% TritonX-100 (Sigma) for 30 seconds. Fixation and permeabilization were monitored on the microscope to minimize disruption of cell membrane contact, based on RICM signal and to ensure preservation of LAT clusters based on TIRF illumination. Antibodies were part of a sampler kit from Cell Signaling Technology (Danvers, MA). All primaries were detected using a goat anti-rabbit Alexa Fluor 647-labeled secondary antibody (Thermo Fisher Scientific, Waltham, MA). Antibodies were incubated for 30-60 minutes at room temperature in PBS in the presence of 1% casein.

Western blotting

A subset of the batch of AND primary T cells used in imaging were lysed in 1% Brij lysis buffer. Cell Signal Technology (#9166 – Rabbit anti-LAT) and Santa Cruz Biotechnology (sc-390394 – Mouse anti-GFP) were used for detection. LICOR IRDye 800CW Goat anti-Rabbit and IRDye 680RD Donkey anti-Mouse were used for secondary detection

Microscopy

Imaging was performed on an inverted Nikon Eclipse Ti-E microscope (Technical Instruments, Burlingame, CA) with a motorized stage (Applied Scientific Instrumentation MS-2000, Eugene, OR), laser illuminator and mercury lamp (Nikon C-HGFIE). A laser

launch (488, 560, and 640 nm diode lasers; Coherent OBIS, Santa Clara, CA) was coupled into a custom fiber (Solamere Technology Group, Inc., Salt Lake City, UT). Laser illumination in TIRF was reflected through a quad dichroic (SPECS) to the objective lens (Nikon 1.47 NA 100x TIRF; Technical Instruments, Burlingame, CA) and collected through appropriate emission filters (ET525/50M, ET600/50M, ET700/75M). Epifluorescent illumination and RICM excitation were selected using a bandpass filters (D546/10x, ET470/40x, ET545/30x, ET620/60x) or a 50/50 beamsplitter, respectively. Filters were from Chroma Technology (Bellows Falls, VT). All emission was collected on an EM-CCD detector (iXon 897DU; Andor Inc., South Windsor, CT). The microscope system was controlled using MicroManager(Cognet et al., 2014).

Imaging Conditions

Interfacial area was measured using RICM; this channel was used to detect initial membrane contact based on visualization of a small, dark feature. pMHC ligand densities were measured using short, 20-30 ms exposures and high incident laser power (30 mW at the source). Bound TCR:pMHC complexes were detected using long, 500 ms exposure times at lower power densities of 0.5 mW (as measured at the objective). Typical intervals between acquisitions were 3 or 10 seconds, depending on the mean dwell time for the agonist peptide. LAT-eGFP was typically imaged with 50-100ms exposures with 0.4 mW of power at the objective. NFAT translocation was visualized using epifluorescence detection at 30-60 second temporal resolution at 3 and 6 microns above the coverslip. Following exposure to the bilayer, cells were imaged up to 30 minutes.

Image Analysis

Image processing was implemented with Python and MATLAB (The Mathworks; Natick, MA) as well as the DIPImage toolbox (Luengo Hendriks, 1999). Single particle tracking of ligated receptor complexes and LAT assemblies was performed using previously described approaches (O'Donoghue et al., 2013 and Low-Nam, et al., 2011). We also used TrackMate (Tinevez et al., 2017) to track events of interest.

Contact area and cellular boundaries were extracted based on the LAT or RICM signature. Briefly, the intensity histogram for RICM images was plotted and the lower values of the bimodal distribution represented the cell area. The histogram was used to threshold raw images and used as the basis for a mask. Cellular activation was set based on the first detection of NFAT in the nucleus and was quantified as described previously (Lin et al., 2019).

2 | PLC-γ1 controls timing of LAT condensations localized to single TCR.

Abstract

T cells discriminate between self and agonist peptides by requiring long dwelling binding events between peptide-MHC and the T Cell Receptor (TCR). A consequence of successful signal transduction is the formation of a multi-molecular assembly of downstream molecules that is crosslinked by the phosphorylated scaffold protein Linker for Activation of T cells (LAT). While the general sequence of events leading to LAT assembly has been studied in detail, no study has measured the distribution of cellular response times relative to individual ligation of the TCR. Such measurements produce valuable insight into the antigen discrimination process. Using a supported lipid bilayer platform and TIRF microscopy, we directly measure the intracellular responses to single pMHC-TCR binding events in living primary T cells with high spatiotemporal, multi-color resolution. This provides the ability to accurately determine the order of events in TCR signal transduction in relation to a single TCR, as opposed to bulk stimulation methods. We observe that after a pMHC binds to a TCR that LAT condensation occurs after an extended delay of approximately 25 seconds. While this timing is likely set, in part, by a competition of kinase/phosphatase pressure and LAT diffusion, detectable LAT phosphorylation does not occur until the assembly begins to form. This suggests that diffusive phospho-LAT requires an additional event to trigger aggregation. We find that phospholipase C gamma 1 (PLCγ1) may play a crucial structural role in nucleating LAT condensation. These data demonstrate novel roles for key signaling proteins and, in contrast to ensemble methods, are the first to visualize the decisive steps leading to LAT condensation and completion of kinetic proofreading.

Introduction

The adaptive immune response is initiated by T cells scanning the surface of Antigen Presenting Cells (APCs) seeking to find agonist peptides presented by major histocompatibility complex (peptide-MHC; pMHC). Within this synapse, thousands of T Cell Receptors (TCRs) bind to thousands of pMHC molecules. However, APCs are expected to only display 1-10 agonist pMHC (Demotz et al., 1990; Velazquez et al., 2001). This also parallels the observed sensitivity of the T cell, which can respond to as few as 1-10 pMHC (Huang et al., 2013; Irvine et al., 2002). The primary feature distinguishing agonist peptides from non-agonist peptides is the expected dwell time of interaction with the TCR (Cole et al., 2007; Matsui et al., 1994; Robert et al., 2012; Siller-Farfán and Dushek, 2018). The conceptual framework for a set of molecular interactions that increases downstream sensitivity to a particular dwell time is called kinetic proofreading. This framework has been widely accepted to apply to the TCR (Chakraborty and Weiss, 2014; Germain, 2010; McKeithan, 1995), however the specific molecular logic used by the T cell to sense long dwelling binding events is poorly understood. Moreover, understanding the kinetics of downstream molecular events is crucial to understanding how the T cell discriminates antigen. For a simplest example of how kinetics can effect discrimination see Supplemental Analysis – Markov Scheme.

Signal transduction via kinetic proofreading relies on the slow appearance of kinetic intermediates that are sensitive to the unbinding of the ligand. Originally, the slow forward steps were believed to be phosphorylation of TCRζ that were rapidly reversed if the pMHC unbound the TCR. However, the existence of some phospho-TCRζ prior to stimulation has led to alternative hypotheses (Chakraborty and Weiss, 2014). Recently, Stepanek et al. found evidence that bound TCR:pMHC complexes are slow to find an active LCK molecule. After TCR:pMHC binding, LCK increases the phosphorylation the ζ-chains of the TCR, allowing the recruitment of more ZAP-70 to bind directly to the TCR complex. In addition, LCK phosphorylates and activates ZAP-70. The primary substrate of ZAP-70 is the flexible scaffold protein Linker for the Activation of Thymocytes (LAT). Phosphatases are known to pressure the TCR, and the early sequence of steps towards activation may require phosphatase exclusion in order to proceed. Four tyrosines on LAT are believed to participate in downstream signaling, the distal 3 (Y171, Y191, Y226, see Figure 1) are capable of binding to Growth Factor Receptor Bound Protein 2 (GRB2) as well as GRB2-related Adaptor Downstream of Shc (GADS) (Houtman et al., 2006; Huang et al., 2017). The remaining tyrosine (Y132) plays a crucial role in signal transduction by binding an SH2 domain of PLCγ1, that subsequently activates the Ca^{2+} and DAG pathways. Moreover, ZAP-70 phosphorylates Y132 more slowly than the other phospho-sites (Shah et al., 2016) and it is also believed to significantly contribute to kinetic proofreading (Lo et al., 2019). Direct measurement of these slow steps in vivo has not yet been observed.

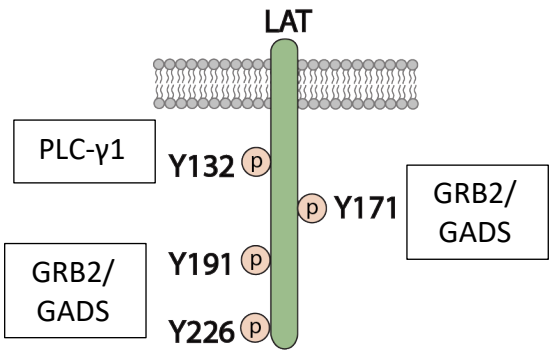

Figure 2-1. Key phosphorylation sites on LAT.

The multivalency of LAT combined with its ability to cross-link via GRB2:SOS:GRB2 leads to the oligomerization of large assemblies of LAT (Houtman et al., 2006; Kortum et al., 2013) (Figure 2). These assemblies exhibit characteristics of phase separation such as condensation and preferred molecular composition (Su et al., 2016). In vitro experiments reveal the condensed phase of LAT to resemble an entangled polymer (Bunnell et al., 2002; Houtman et al., 2006; Huang et al., 2016, 2017a; Li et al., 2012; Su et al., 2016). The condensation of LAT is hypothesized to have signaling consequences by lengthening the dwell time of downstream molecules (Huang et al., 2016) and excluding negative regulators such as phosphatases (Su et al., 2016). Measuring the in vivo kinetics of LAT condensation has had varying results depending on the experiment. Huse et al. used a photoactivable pMHC and measured LAT condensation (via GRB2 recruitment) to be as fast as 7 seconds (Huse et al., 2007). While Yi et al. measured the kinetics of downstream events in Jurkat cells relative to upstream clustering events (Yi et al., 2019). One similarity with both experiments was the use of protein coated coverslips, which stimulate at least hundreds of TCR within a short period of time. The observed kinetics in such experiments are the mean downstream response times convolved with the on-rate of binding within the particular experiment. Both the kinetics as well as amplitude of response per binding event is likely to differ for low-density isolated pMHC binding events.

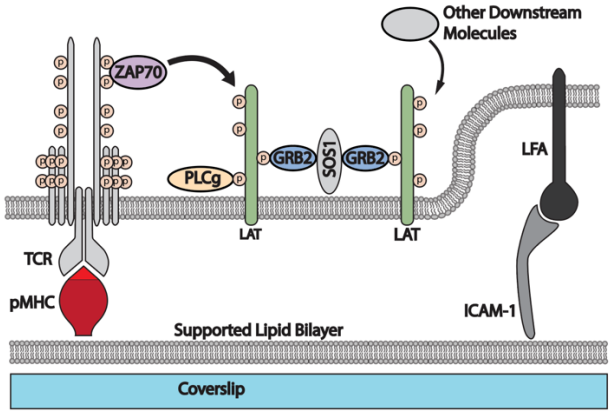

Figure 2-2. Experimental Setup and molecules participating in LAT condensation.
Ligation of the TCR causes LCK to phosphorylate the TCR, allowing ZAP-70 to recruit and in turn be phosphorylated and activated by LCK. ZAP-70 phosphorylates LAT allowing for downstream molecules to bind. GRB2 is known to bind to the three distal phosphorylation sites and can participate in crosslinking LAT with SOS molecules.

Here, we investigate the mechanism and kinetics of LAT condensation relative to the ligation of individual TCR:pMHC binding events. Using a supported lipid bilayer (SLB) we are able to distinguish free-unbound pMHC from TCR-bound pMHC by its dramatic change in mobility (O'Donoghue et al., 2013a). LAT is observed to regularly condense in response to a single isolated TCR:pMHC binding event. After a long delay of no activity, the LAT will condense suddenly. This is indicative of some type of nucleation event enabling the rapid growth of the LAT assembly. Measuring the delay times of ZAP-70, GRB2, and PLC-γ1 relative to ligation reveals the distributions of events downstream of single binding events, which are fundamental relationships needed to understand the integration of signaling within T cells. We discover a previously unappreciated role of PLC-γ1 in nucleating the LAT assembly which suggests that the condensation of the LAT assembly gates downstream signaling. These data demonstrate novel roles for key signaling proteins and, in contrast to ensemble methods, are the first to visualize the distributions of downstream events leading to LAT condensation and completion of kinetic proofreading.

After a long delay, LAT condenses suddenly, near long lived TCR:pMHC binding events

Here we use single-molecule imaging to track binding events between pMHC and TCR (Lin et al., 2019; O'Donoghue et al., 2013b), with the aim of measuring how individual binding events (Figure 3A) contribute to the condensation of LAT (Figure 3B). To track the proximal signal from binding events requires the binding to be long enough

to pass kinetic proofreading. At the single molecule level each TCR will have its own threshold to activation, and in order to capture the range of responses requires using a "long-dwelling" agonist. SPR measurements of cognate pMHC-TCR pairs suggest that a typical agonist dwell-time is on the order of 2-15 seconds (Cole et al., 2007). Imaging single molecule dwell-time measurements on the OT-I system found the minimum average dwell time for stimulation to be 1.9 sec, while robust stimulators, capable of stimulating at low densities, tended to have an average dwell-time of 10-20 sec (Stepanek et al., 2014). Another recent study suggests that downstream T cells activation, as read out by NFAT, tends to be tuned to long dwelling events (> 30 seconds) (Lin et al., 2019). In order to sufficiently sample the long dwelling events and the range of TCR responses we primarily used the AND(TCR):MCC(peptide) system, which has an expected dwell time of ≈46 sec (O'Donoghue et al., 2013b). This allows us to observe both short and long binding events. The same qualitative results in this study can be seen with shorter binding agonists (e.g. T102S, data not shown), albeit with dramatically reduced frequency.

The T cells are deposited onto a supported lipid bilayer (SLB) functionalized with adhesion and simulation. The SLB was doped with Ni^{2+}-chelating lipids that allows the stable association of histidine-tagged intercellular adhesion molecule-1 (ICAM-1) and histidine-tagged MHC class II (IE^k) (Nye and Groves, 2008). Prior to adding MHC to the bilayer, it was loaded with Atto647N-tagged MCC peptide. This and other dyes have been used in similar experiments with no measurable difference on TCR:pMHC binding kinetics (Lin et al., 2019). The pMHC densities used in this study were 0.05 - 0.15 μm^{-2}. Low densities were used for two reasons. For practical reasons, low densities are required to be able to reliably distinguish single molecule binding events from each other. In addition, it is known that a handful of agonist pMHC are sufficient to drive T cell activation (Huang et al., 2013; Irvine et al., 2002).

Individual pMHC molecules were imaged with total internal reflection fluorescence (TIRF) microscopy. Without T cells present, the pMHC are observed to undergo 2D Brownian motion, with a diffusion coefficient of 0.56 μm^2/mol (Supplemental Analysis – Diffusion) and appear as a homogenous population. After T cells are added, some pMHC will slow down dramatically for a period of time, then resume typical diffusive motion. This change in diffusion is a clear mark of binding for two reasons – it is specific to agonist pMHC (O'Donoghue et al., 2013b) and it produces localized intracellular responses specific for the TCR. A 500 ms exposure was used to visually distinguish the bound and unbound populations of pMHC. Binding events and LAT clusters were tracked with semi-automated and manual tracking with TrackMate (Tinevez et al., 2017).

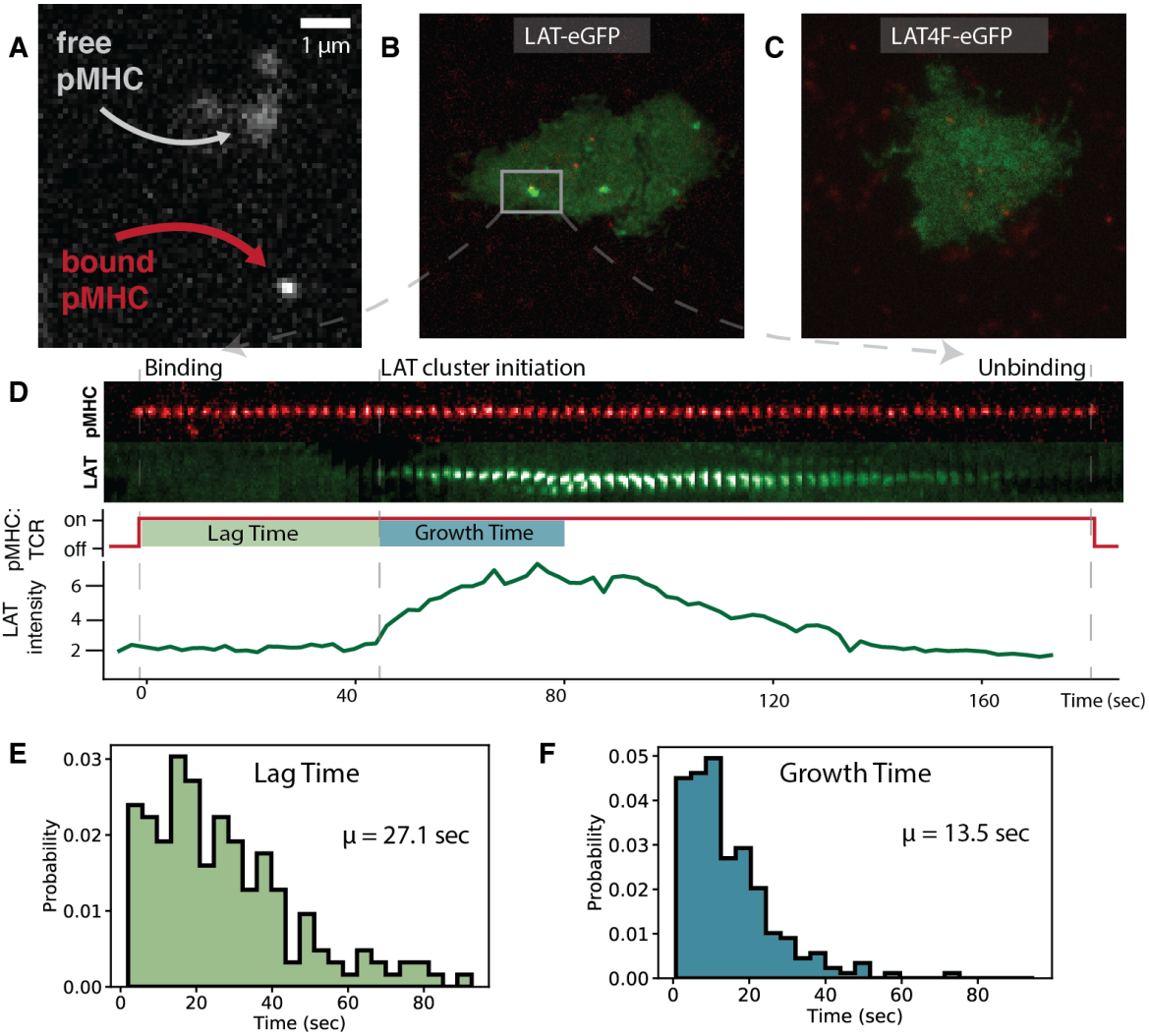

Figure 2-3. After long delay, LAT condenses suddenly.
(A) Atto647N labeled MCC peptide is loaded into his-MHC and deposited onto the bilayer, along with his-ICAM-1, on a 2% Ni-DGS bilayer. The fluorescent MCC-MHC is visualized at 500 ms exposure while under a T Cell. Bound pMHC is readily resolvable from unbound free pMHC. (B) At low pMHC densities (≈ 0.08 μm^{-2}) LAT is regularly observed to condense near TCR:pMHC binding events. LAT condensates appear sparse at low ligand densities. (C) LAT with the four signaling tyrosines mutated to phenylalanine. No condensates are visible. (D) Time series image of binding event called out in (B). Top: Atto647 pMHC binding a TCR. Bottom: LAT condensation colocalized with the binding event. The key events of ligand binding, LAT cluster initiation, and ligand unbinding are all clearly resolvable. Two parameters of interest are the lag time, measured from the initiation of binding to the first detectable frame of LAT condensation, and the time for the LAT cluster to reach its maximal size (growth time). (E) Histogram of lag times from binding events across 12 cells. (F) Histogram of growth times from those same 12 cells.

Peripheral CD4+ T cells from transgenic AND TCR mice were retrovirally transduced with LAT-eGFP and deposited onto the bilayer. At low ligand densities, transient condensates of LAT were observed to regularly colocalize with TCR:pMHC binding events (Figure 3B and 3D). These condensates represent a large amplification of

signal, and it is informative that this node of the pathway is sensitive to a single binding event. The size and extent of LAT condensation is dramatically different than seen in bulk studies (Bunnell et al., 2002; Houtman et al., 2006), this shows that LAT is capable of scaling the response of the cell from single binding events up to much higher concentrations. These condensates are a specific function of the 4 distal tyrosines (murine LAT: Y136, Y175, Y195, Y235) since mutation to phenylalanine abolished the condensate phenotype (Figure 3C).

We examined the kinetics of LAT condensation relative to the start of TCR ligation with pMHC (Figure 3D). This is the first measurement of the distributions of proximal T cell signaling kinetics at the level of a single binding event. Interestingly, we find a broad distribution of lag time between TCR ligation and the initiation of the LAT assembly (Figure 3E). The mean lag time is μ = 27.1 seconds. This long delay represents the sum of slow kinetic steps regulating the initiation of downstream signaling – including finding an active LCK and the accumulation of sufficient phospho-LAT for observable condensation. Initiation of the assembly is followed by fairly rapid growth of the LAT cluster, μ = 13.5 seconds. This discrepancy suggests that the growth of the LAT assembly is non-linear, with some type of positive feedback being a rate limiting step. One could argue that the background signal of LAT-eGFP may obscure an otherwise early start of a linear reaction. However, extrapolating backwards from the observed start, using the observed initial velocity of reaction, will on average intercept the 0 signal axis at 12.1 seconds prior to the observed start, which is significantly shorter than the observed lag time. Therefore, it is unlikely that the assembly of LAT begins shortly after TCR ligation, but rather it exhibits non-linearity associated with either delayed nucleation or positive feedback.

Potential models of condensation.

To understand the cellular mechanism of LAT condensation we seek to find the rate limiting steps necessary for condensation. The long lag time observed (Figure 3E) has at least four straightforward possibilities. The simplest would be that most of the lag time is attributable to the waiting time for ligated TCR to find an active LCK, as has been proposed in the Coreceptor Scanning hypothesis (Figure 4A). The fairly rapid diffusion of LAT may couple with other fast recruitment events to allow for fairly linear growth of the LAT cluster once ZAP-70 is activated. Stepanek et al. estimate that a ligated TCR will find an active LCK:CD4 on the order of ≈2 seconds, while in CD8 T cells the ligated TCR is expected to find an active LCK:CD8 on the order of ≈40 seconds. This is a large range and suggests that, depending on the LCK coupling efficiency of our T cells, this step may subsume the entirety of the lag time we observe.

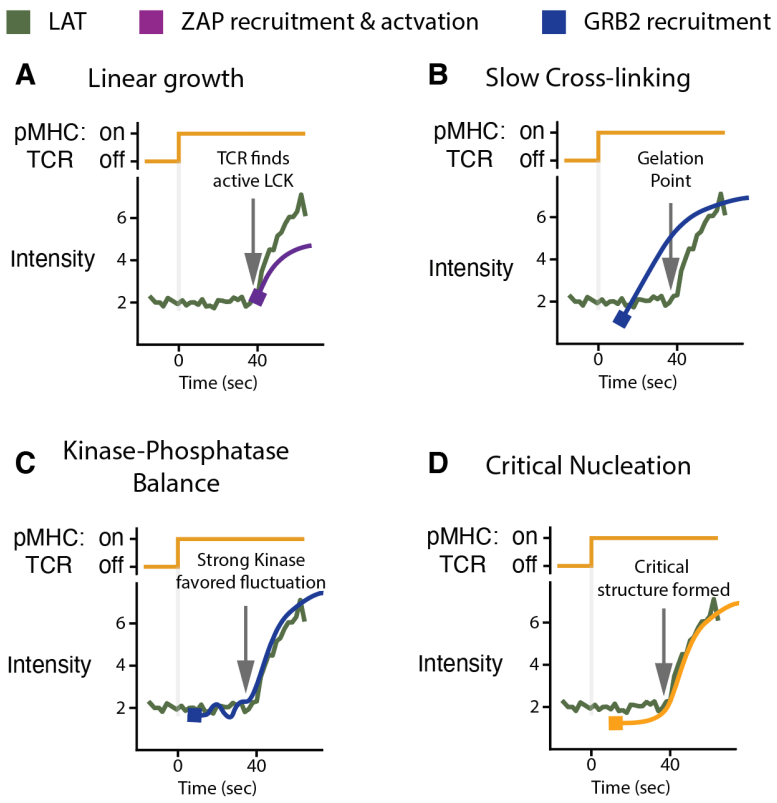

Figure 2-4. Potential rate-limiting steps of LAT condensation.
(A) The simplest explanation of a long lag time would be if the observed growth did not start until ZAP-70 became active, producing linear growth of LAT. (B) Model of diffusion limited condensation of phospho-LAT. Requires early build up of phospho-LAT (read out as GRB2 recruitment). (C) If phosphatase pressure must be overcome a rate limiting step may be a strong kinase fluctuation. (D) Some other type of nucleation event – such as recruitment of another protein or a critical germ nuclei of condensed LAT.

However, if ZAP-70 does activate early, then there exists some other barrier to condensation. Slow cross-linking of phospho-LAT may arise in a variety of ways, but such a process would have clear observables with our experimental approach. GRB2 has a fairly high concentration in cells (Cruz-Orcutt et al., 2014) and its high on-rate should give us a good estimate of the extent of phospho-LAT within a few seconds (Huang et al., 2017a). If phospho-LAT diffuses slowly, then condensation may resemble diffusion limited aggregation (DLA). Some cross-linkers, such as SOS, may recruit slowly. In either of these cases we'd expect to see an early increase in GRB2 that then reaches a critical level that precipitates LAT condensation (Figure 4B). Another potential barrier is phosphatase pressure. One model of early T cell activation is kinetic segregation or "size-exclusion" of phosphatases (Cordoba et al., 2013; Davis and van der Merwe, 2006). Given the short binding of TCR-pMHC relative to the large ectodomain of the CD45 phosphatase, it is thought that TCR:pMHC binding excludes phosphatases and allows for net kinase activity of LCK and ZAP-70. More recently, it has been shown that the LAT condensate itself is capable of excluding phosphatases (Su et al., 2016). In addition to passive phosphatase pressure, activated ZAP-70 kinases compete against the diffusion

of phospho-LAT. If this is limiting LAT condensation, then a strong kinase favored fluctuation is required to begin growth (Figure 4C). Lastly, a delayed start of both phospho-LAT accumulation and condensation could be explained by a more direct event such as the slow phosphorylation of Y136, or the recruitment of other downstream molecules (Figure 4D).

ZAP-70 recruitment is slow but does not fully account for LAT lag time.

To understand the role of ZAP recruitment as a rate limiting step of LAT assembly formation, we imaged its time-dependent enrichment over individually ligated TCR (Figure 5A). Primary AND T cells were retrovirally transduced with fluorescently labeled ZAP-70. There is a small, but detectable increase in fluorescent signal over binding events. This is likely due to non-clustered, i.e. monomeric, TCR driving downstream signaling (Brameshuber et al., 2018; O'Donoghue et al., 2013a; Rossboth et al., 2018). The brighter mNeonGreen fluorescent protein (FP) had a slightly better signal to noise ratio compared to other FPs used. The observed lag time between TCR binding and ZAP had a mean recruitment time of 13.4 seconds. Biochemical studies have seen ZAP-70 become phosphorylated within 15 seconds of bulk stimulation in Jurkats (Chan et al., 1991), and modeling results have estimated that at the single molecule level a ligated TCR will find an active LCK within 2-40 seconds, depending upon the extent of active LCK coupling with CD4/8 coreceptor (Stepanek et al., 2014). The 13.4 second lag time observed in our system represents a significant fraction of the total 27.1 second lag time for LAT condensation, but suggests that the "slow ZAP" model (Figure 4A) is incomplete. In its cytosolic state, ZAP-70 is believed to recruit quickly to phosphorylated TCR (Klammt et al., 2015), and given that the TCR has already found an active LCK it is likely to become quickly activated. It is then puzzling that LAT growth has an additional long delay after ZAP-70 recruitment, especially considering the recently discovered bridging interaction between LCK, ZAP-70, and LAT (Lo et al., 2018). This additional lag may arise from a mixture of kinase-phosphatase balance and/or a wait time for critical nucleation.

GRB2 enriches simultaneously with LAT density transition.

Given the long delay between ZAP-70 recruitment and LAT condensation it was necessary to determine if ZAP-70 product was accumulating within this interim. Primary AND T cells were retrovirally transduced with C-terminally labeled mNeonGreen-GRB2. Expressing just the SH2 domains tends to occlude downstream signaling (unpublished data), so full length GRB2 was used. The observed lag time between TCR ligation and GRB2 recruitment had a mean delay time of 28.2 seconds (Figure 3B). This is comparable to the mean lag time for LAT (27.1 seconds) and suggests they arrive in a concerted fashion. GRB2 background fluorescence was less homogeneous than the membrane bound LAT. With a bright FP such as mNeonGreen we are able to detect 5-15 colocalized GRB2 molecules (Supplemental Analysis – GRB2 Sensitivity), and this should provide reasonable detection of fluctuations in phospho-LAT.

To verify the concerted recruitment of GRB2 and condensation of LAT we utilized a P2A self-cleaving peptide to simultaneously express LAT-mScarleti and mNeonGreen-GRB2 at equimolar amounts (Liu et al., 2017). In each instance of ligated TCR producing GRB2 and LAT assembly, the GRB2 and LAT signals appeared simultaneously (Figure 5C). While streaming the formation of the LAT assembly, with ≈200 ms resolution, there wasn't any discernable delay between GRB2 enrichment and LAT condensation. This concerted appearance of GRB2 and LAT is *inconsistent* with "slow-crosslinking of GRB2-LAT" (Figure 4B) being a major bottleneck to the initiation of the assembly.

The delay between ZAP-70 and GRB2/LAT could potentially be explained by phosphatase pressure. Using orthovanadate, a broad inhibitor of tyrosine phosphatases, we did not detect any noticeable change in lag time (Figure 5E) or LAT assembly size, consistent with other results using orthovanadate (Park et al., 1991). SHP2 is a ubiquitously expressed phosphatase that is believed to recruit to phosphorylated RTKs, cytokine receptors, and/or scaffolding adaptors (Chan et al., 2008). Treatment of cells with SHP099, a specific allosteric inhibitor of SHP2 (Fortanet et al., 2016), did not significantly accelerate the condensation of LAT. Even though we did not observe a direct effect of phosphatase inhibitors, we do see fluctuations of GRB2 and LAT condensation (Figure 5D). Most binding events either fail to produce any signal or produce assemblies of hundreds of LAT molecules (see Chapter 1). However, a small subset show local intracellular fluctuations in response to binding events. This suggests there are pressures working against the condensation of LAT. A possible explanation is the presence of an untested phosphatase such as CD148 (Chakraborty and Weiss, 2014), another possibility is the diffusion of pLAT away from the active site, or active ZAP itself diffusing away from the site of ligation (Katz et al., 2016).

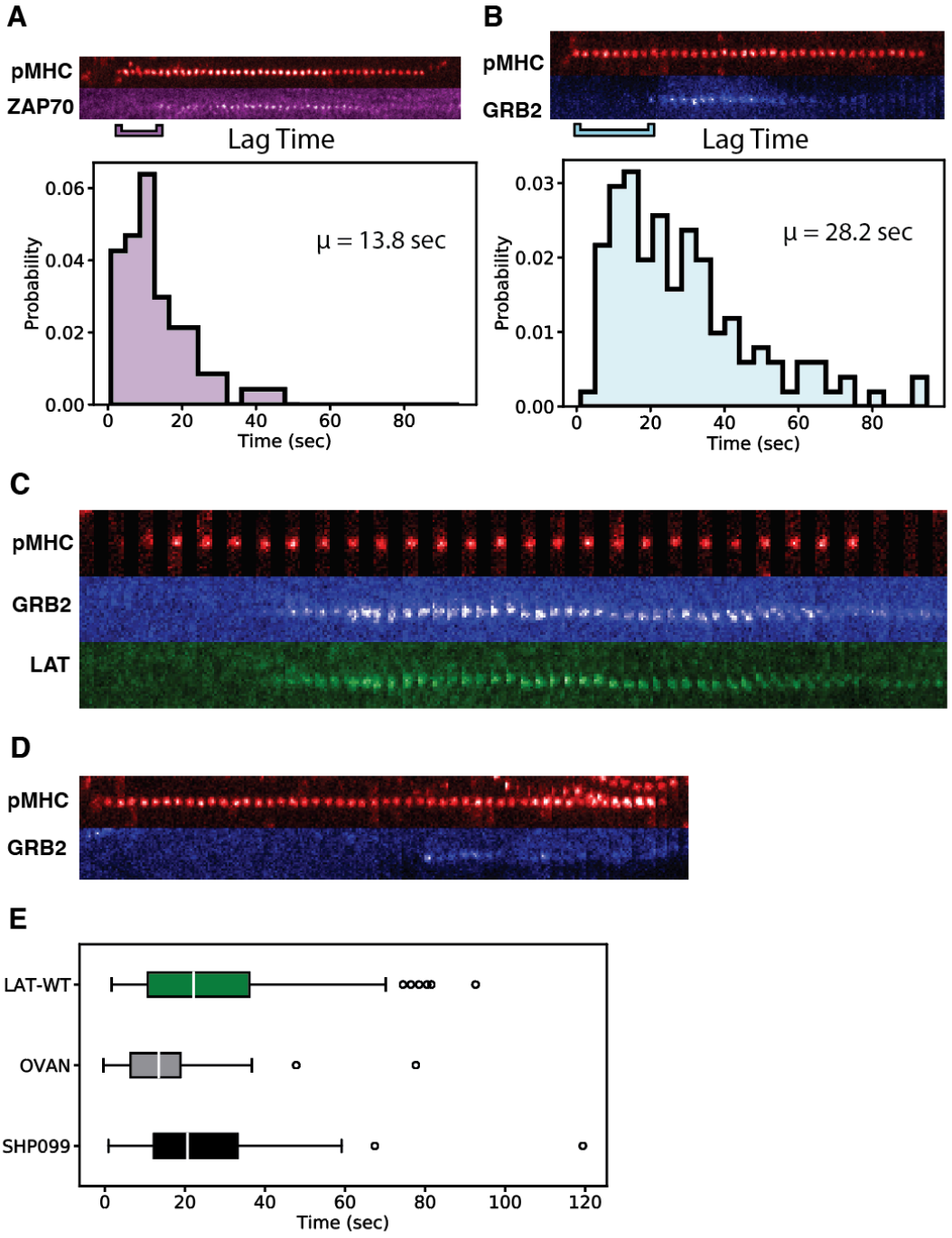

Figure 2-5. ZAP-70 is slow, but not as slow as GRB2 or LAT.
(A) Top: Time series images of ZAP-70-mNeonGreen recruitment to singly ligated TCR. Bottom: Histogram of observed lag times between TCR:pMHC binding and ZAP-70 recruitment. (B) Top: Time series images of GRB2-mNeonGreen recruitment to a single ligated TCR. Bottom: Histogram of observed lag times between TCR:pMHC binding and GRB2 recruitment. (C) Time series images of primary T cells expressing both GRB2-mNeonGreen and LAT-mScarleti. (D) Time series images showing fluctuations of GRB2 recruitment to a ligated TCR. (E) Boxplot comparing lag times of condensation with orthovanadate (OVAN) and SHP099 phosphatase inhibitors with wild type LAT.

Recruitment of PLC-γ1 triggers condensation.

To expand the scope of our study, we sought to find the recruitment kinetics of PLC-γ1. Even though PLC-γ1 has many membrane binding domains, LAT is necessary for its recruitment to the membrane (Yi et al., 2019). Previous studies have shown that phosphorylation of PLC-γ1 has a significant delay after the phosphorylation of LAT-Y191 and initiates at the same time as LAT-Y132 (Cruz-Orcutt et al., 2014). Given the much slower rate of Y132 phosphorylation by ZAP-70 compared the other sites on LAT (Huang et al., 2017a; Lo et al., 2019) , we expected to find PLC-γ1 arrive after the condensation of LAT. However, expressing PLC-γ1 and LAT in T cells showed accelerated recruitment relative to LAT, with a mean recruitment time of 16.2 seconds (Figure 6B).

The accelerated appearance of PLC-γ1 relative to the condensation of LAT could mean there is an additional lag time between the arrival of PLC-γ1 and the condensation of LAT. But it is more likely the case that PLC-γ1 co-occurs with LAT condensation and that its overexpression merely increases the rate at which PLC-γ1 recruitment triggers condensation of the LAT assembly. Determining which of these two possibilities occurs requires the examination of dual PLC-γ1 / LAT expressing cells. Given the large size of full-length PLC-γ1, retroviral transduction with a PLC-γ1-P2A-LAT proved unsuccessful. Rather, we transduced primary AND T cells with separate PLC-γ1-mNeonGreen and LAT-mCherry viral particles and then sorted for high expressing cells. The LAT-mCherry signal to noise ratio was very low but was nonetheless strongly time-correlated with PLC-γ1-mNeonGreen (Figure 6A). We found that PLC-γ1 arrives simultaneously with LAT condensation within the error of our measurements, ± 1 seconds.

To determine whether PLC-γ1 had a mechanistic role in triggering the condensation, as was suggested by the lag time observations, we examined a G135D LAT-eGFP mutant. It was recently found that the human analog G131D significantly speeds up the rate of ZAP-70 phosphorylation of Y132 (Shah et al., 2016). If this phosphorylation event facilitated LAT condensation, then increasing its rate of reaction should shorten the observed lag time to condensation. G135D LAT-eGFP was retrovirally transduced into primary AND T cells. The mean lag time between TCR:pMHC binding

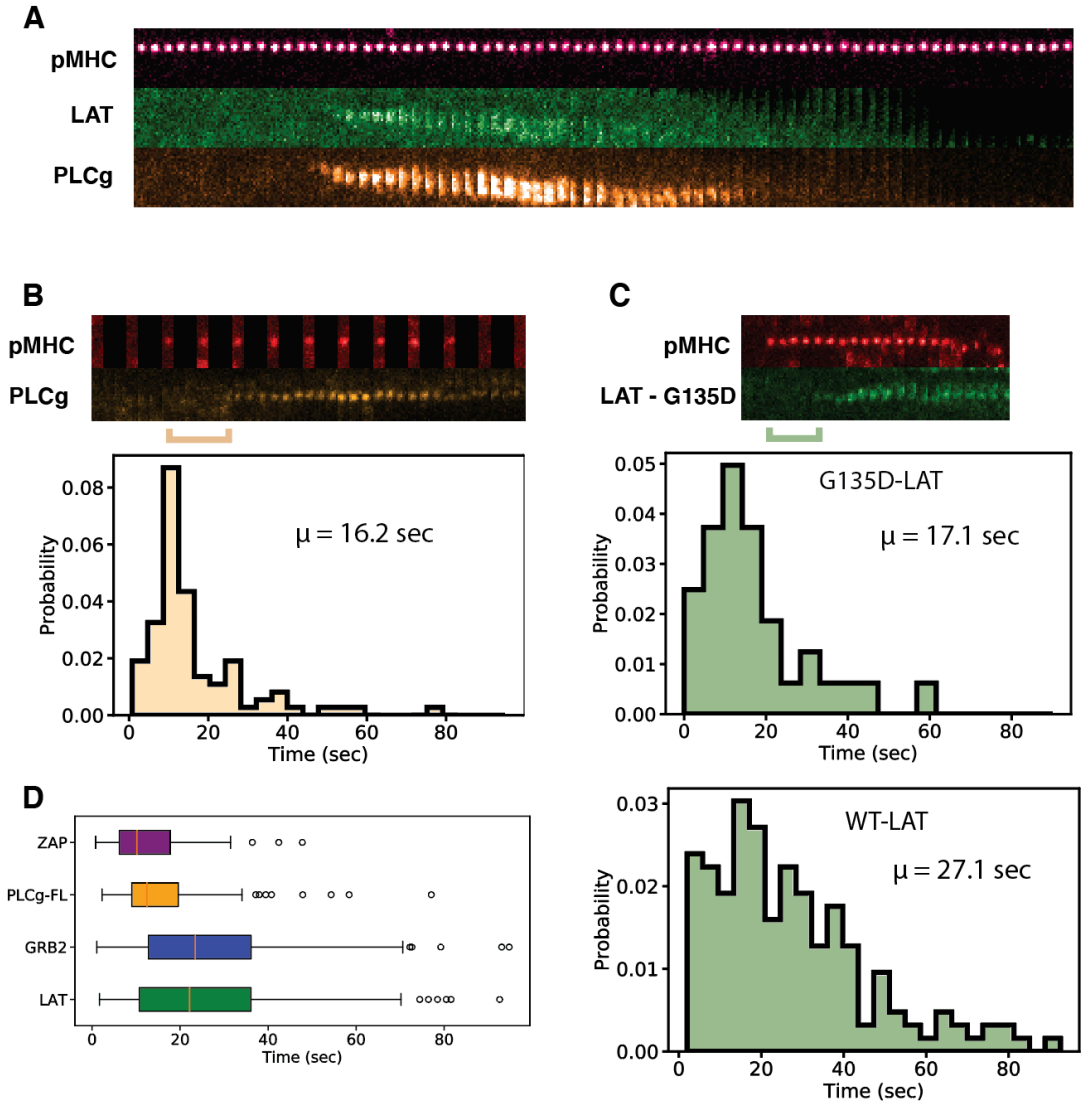

Figure 2-6. Recruitment of PLC-γ1 triggers LAT condensation.
(A) Time series images from a primary T cell expressing both LAT-mCherry and PLC-γ1-mNeonGreen showing simultaneous recruitment of PLC-γ1-mNeonGreen and condensation of LAT-mCherry relative to a TCR:pMHC binding event. (B) Top: Time series images of PLC-γ1-mNeonGreen recruitment to a singly ligated TCR. Bottom: Histogram of observed lag time between TCR:pMHC binding and PLC-γ1 recruitment. (C) Histogram of observed lag time between TCR:pMHC binding and the condensation of G135D LAT-eGFP. Below is the histogram of lag times for WT-LAT. (D) Boxplot comparison of lag times of different molecules examined in this study.

and LAT condensation in these conditions was 17.1 seconds, which is significantly faster than WT-LAT (Figure 6C). Given that PLC-γ1 and LAT seem to arrive simultaneously (Figure 6A), it is then informative that the overexpression of PLC-γ1 accelerates the condensation. Together this suggests that recruitment of PLC-γ1 controls the timing of the condensation of LAT and that there are two comparably strong components to its recruitment rate – the phosphorylation of Y136 and the concentration of PLC-γ1.

Discussion

The dynamic properties of intracellular responses have been difficult to quantify, in large part due to the difficulty in timing the initiation of the signaling cascade. By observing isolated TCR:pMHC binding events in space and time we are able to measure the dynamics of cellular outputs towards the most basic of cellular inputs – a single receptor-ligand binding event. In this study we measured the lag times between individual TCR:pMHC binding events and subsequent downstream outcomes. The ability to define the moment of engagement while keeping the cell far from receptor saturation allows us to observe the dynamics that lead up to cellular activation as opposed to the dynamics of saturated cellular responses. Moreover, the kinetics at the single molecule level are crucial in governing the sensitivity of the T cell to dwell time and its capacity to discriminate antigen.

We find that the time between TCR:pMHC ligation and LAT condensation has a broad distribution that is centered around 27.1 seconds. This total transit time can be decomposed into at least three dominant kinetic bottlenecks. First, there is a long delay until ZAP-70 recruitment (13.4 seconds). This observation is consistent with some form of Coreceptor Scanning and suggests that the delay of increased ZAP recruitment plays an important role in controlling the initiation of T cell signaling. The second and third bottlenecks are the slow phosphorylation of Y132 and the subsequent recruitment of PLC-γ1 respectively. Deconvolving the last two steps is difficult, especially due to the effects of overexpression in our system. Of interest is the fact that the lag time between TCR ligation and ZAP-70 is only 3 seconds faster than the lag time between TCR ligation and PLC-γ1 (when overexpressed).

Other studies examining kinetics have mostly been at high levels of stimulation, with even low-doses still likely stimulating hundreds of TCR. Huse et al. were able to precisely control initiation by having a photoactivatable agonist (Huse et al., 2007). Even though uncaging of the pMHC occurs within 1 ms, the on-rate of pMHC binding to TCR is unsynchronized. Nonetheless, this approach of controlled initiation coupled with a large stimulus has given valuable insight into the maximum rates of downstream events. They found recruitment of GRB2 and subsequent DAG production (PLC-γ1 product) to occur at ≈4 and 8 seconds respectively. The more rapid kinetics observed by Huse et al. is explained by the fact that this experiment is tracking the fastest response of hundreds of receptors, whereas our experiment is measuring the distribution of responses to individually triggered receptors. In line with Huse et al., Cruz-Orcutt et al. found that PLC-γ1 becomes activated after phosphorylation of LAT-Y191 (Cruz-Orcutt et al., 2014). They observe PLC-γ1 becoming activated at a similar delay as the phosphorylation LAT-Y132, beginning at ≈15 seconds. After initiation, pY132 is observed to increase slowly, whereas phosphorylated PLC-γ1 has a highly cooperative response. Our imaging study suggests that the origin of this cooperative response may lie in the condensation of the

LAT assembly as triggered by PLC-γ1 recruitment. The molecular organization that occurs during condensation may be responsible for the activation of PLC-γ1. It appears that the only path for PLC-γ1 to initially recruit to the membrane is via LAT, as shown with LAT KO Jurkats (Yi et al., 2019). In addition, Yi et al. were able to measure mean lag times by comparing the clustering of downstream molecules relative to clustering of upstream molecules. At 37°C they found the lag time between TCRζ clustering and ZAP-70 clustering to be ≈10 seconds, while the lag between ZAP-70 clustering and GRB2 recruitment to be ≈14 seconds. Together, the observed lag time between TCRζ clustering and the appearance of GRB2 would be ≈24 seconds. Even though this is superficially close to our measurement of lag time between TCR ligation and GRB2 appearance, the measurement of Yi et al. does not include the delay time between TCR ligation and TCR clustering (t=0 for their measurements). Another interesting observation of Yi et al. was an increase in lag time of ZAP-70 with TCR clustering start time, presumably due to an increases of calcium; however, we do not observe such a trend with our experiments (Supplemental Analysis – Lag Time Correlations). This is likely due to the fact that our experiments are at much lower levels of stimulation (~0.05 mol/μm^2) and are unlikely to stimulate calcium (Lin et al., 2019). In addition, our experimental approach is sampling the broad distribution of single molecule responses, whereas the approach in Yi et al. looks at the ensemble response of hundreds of molecules.

We find that cells overexpressing PLC-γ1 have a shorter delay time between TCR ligation and PLC-γ1 recruitment than the delay time between TCR ligation and LAT condensation. Cells dually expressing PLC and LAT show similar lag times for both LAT and PLC assembly relative to TCR binding. These data suggest that PLC-γ1 has a role in accelerating the condensation of LAT. Structurally, SOS is considered the primary cross-linker of LAT. SOS induced oligomerization of LAT is thought to occur via ≈2:1 GRB2:SOS stoichiometry extending the ≈3:1 GRB2:pLAT valency (Houtman et al., 2006). In vitro experiments have shown this is sufficient to form an extended gel phase (Huang et al., 2016; Su et al., 2016). Though the scaffold function of SOS is important, SOS -/- cells merely showed diminished pLAT clustering (Kortum et al., 2013), suggesting that SOS may be a primary cross-linker, but that other interactions of downstream molecules may also contribute to cross-linking. The ability of PLC-γ1 to cooperatively assemble GADS:SLP-76:PLC:LAT (Manna et al., 2018), potentially in trans with LAT, coupled with GADS dimerization, which can also bind the three distal tyrosines on LAT (Houtman et al., 2004; Sukenik et al., 2017), may help facilitate further growth of the LAT assembly.

Lastly, our data suggest that the rate of *recruitment* of PLC-γ1 may play a role in antigen discrimination. When Y132F mutants were introduced into LAT knockout Jurkats (Houtman et al., 2006), they found Y132F to not be necessary for clustering, however in these experiments bulk stimulation of thousands of kinases likely overcame any need for PLC-γ1 nucleation. Interestingly, it has been shown that in vitro stimulation of T cells leads to a 75 fold increase in PLC-γ1 expression (von Essen et al., 2010), and PLC-γ1 has been observed to be expressed at such high levels in Jurkats as to be 1:1 with GRB2

(Cruz-Orcutt et al., 2014). This suggests that PLC-γ1 expression level is one way effector T cells may tune their activation to be more sensitive to agonist than naïve cells (Iezzi et al., 1998).

In conclusion, typical sigmoidal traces seen in almost all kinetic experiments are a synthesis of discrete stochastic events. By measuring the downstream responses to individual receptor-ligand binding events, we can directly measure the distribution of these stochastic events. This includes the probabilities of occurrence as a function of time as well as the inter-delay times ("deltas"). By measuring these distributions, we can understand the stochastic signal trajectory from an individual TCR. Using this approach, we were able to measure the kinetic delay time distributions of multiple crucial steps in the T cell signaling pathway. And we found that at low pMHC densities, PLC-γ1 may have an unappreciated role in nucleating the LAT assembly.

Supplemental Analysis – Markov Scheme

Background

The simplest kinetic scheme that gives rise to kinetic proofreading is a cycle (Ge et al., 2012) that includes a molecule capable of forming an intermediate that can be escaped in a manner similar to the ground state molecule. To provide a simple illustration, consider a TCR bound by pMHC in a state C_1. Structural studies suggest that foreign and self-peptides produce similarly structured TCR. Given this, both foreign and self-peptides are capable of generating state C_1. We make the simplification that there are generally two states accessible from C_1, either the ligand unbinds the TCR, producing state L_1, or a new signaling state C_2 is achieved. Both of these transitions occur with an off-rate or forward-rate respectively. The important step for proofreading relies in C_2 also being revertible to state L_1 (L_1 = unbound TCR and Ligand). The simplest mathematics follows if we allow the off-rates and forward-rates to be constant, when in reality each state transition rate is likely different.

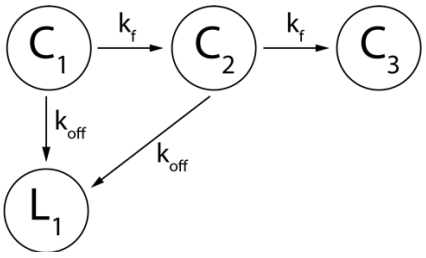

Modeled as a continuous Markov chain yields the following transition matrix:

$$\begin{pmatrix} -(k_f + k_{off}) & k_f & 0 & k_{off} \\ 0 & -(k_f + k_{off}) & k_f & k_{off} \\ 0 & 0 & 0 & 0 \\ 0 & 0 & 0 & 0 \end{pmatrix}$$

With the following limiting probability distribution:

$$p = \begin{pmatrix} 0 \\ 0 \\ \dfrac{k_f^2}{(k_f + k_{off})^2} \\ \dfrac{k_f k_{off}}{(k_f + k_{off})^2} + \dfrac{k_{off}}{(k_f + k_{off})} \end{pmatrix}$$

In the limit of a slow k_f then:

$$p(C_3)/p(L_1) = (k_f/k_{off})^2$$

And the relative probability of C_3 for two different off rates becomes:

$$p(C_3; k^1_{off})/p(C_3; k^2_{off}) = (k^2_{off}/k^1_{off})^2$$

The above result is the classic result of Hopfield (Hopfield, 1974) and Ninio (Ninio, 1975) and it suggests that a single kinetic intermediate can at most square the discrimination between ligands.

Supplemental Analysis – Diffusion

$$\langle r \rangle = \sqrt{Dt}$$

From the fundamental equation above and a diffusion coefficient of D=0.56 μm^2 s^{-1} can deduce that at short exposures, for example 20 ms, a pMHC is expected to move ≈100 nm while having ≈40 nm of uncertainty in position (due to localization error). This positional uncertainty is a significant fraction of the travel distance. Though we have much more statistics when we include all steps, the accuracy improves as the particles traverse greater distances. For this reason, we use a single fit parameter D to fit multiple time-delayed 2D step-size distributions. The 2D step-size distribution is mathematically equivalent to the chi distribution. In the case for the figure below we sampled positions at 80 ms (blue), 160 ms (orange), and 320 ms (green).

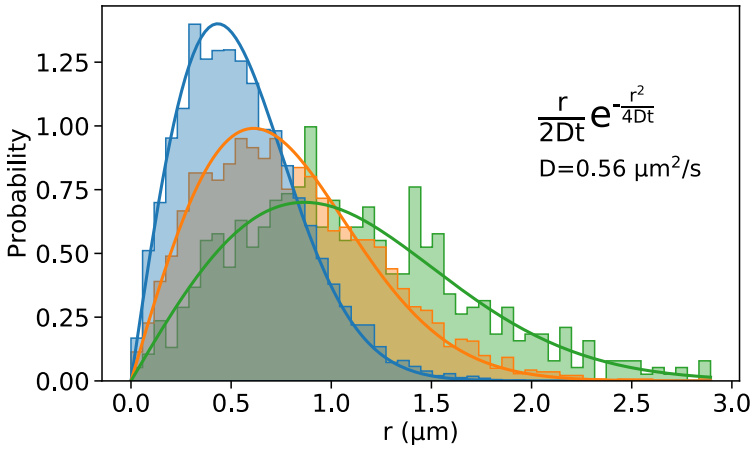

Figure 2-7. Step-size distribution of freely diffusing of pMHC. Atto647-labeled pMHC on 2% Ni-DOGS 98% DOPC bilayers at 37 °C.

Supplemental Analysis – GRB2 Sensitivity

We are interested in the approximate number of membrane bound GRB2-mNG molecules in puncta over background GRB2-mNG per μm^2. We applied a recently reported method (Mutch et al., 2007). First, (σ/μ) is calculated for the GRB2-mNG puncta and was found to be much less than the (σ/μ) for the single point-spread function (PSF) distribution. This indicated that the random addition of fluorophores was a good approximation for the observed puncta. Next, "basis histograms", i.e. probability mass functions with bins of interest, were generated from the single PSF distribution by performing multiple convolutions. Finally, the distribution of puncta intensities was deconvolved into coefficients of the "basis histograms".

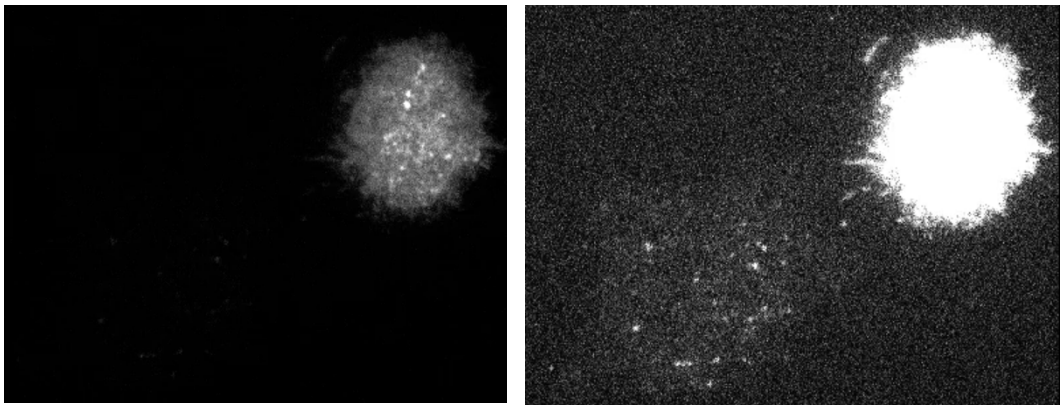

Figure 2-8. mNeonGreen-GRB2 single-molecule distribution to measure puncta.
(left) Image of two cells with the contrast optimized for the higher-expressing cell
(right) Image of the same two cells, but with the contrast optimized for the single-molecule density cell.

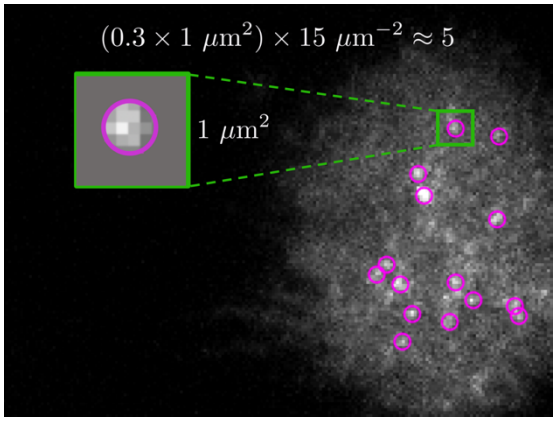

Figure 2-9. Estimation of number of GRB2 in puncta.
Average signal over background is approximately 0.3 giving a mean number of 5 GRB2 molecules concentrated within the puncta region.

Supplemental Analysis – Lag Time Correlations

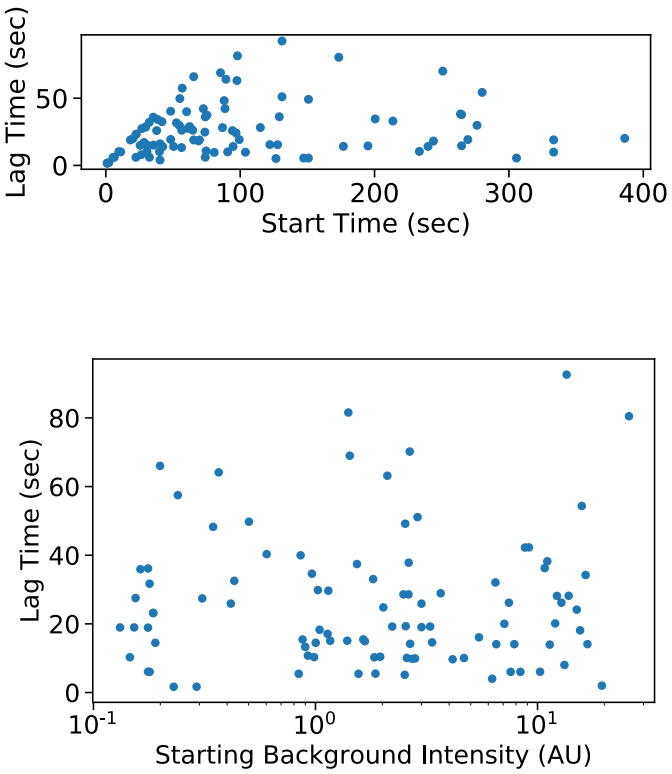

Figure 2-10. Scatter plots of potential correlates with lag time of LAT condensation.
(a) The start time of the cluster is the time of initiation relative to the start of the acquisition.
(b) The starting background intensity is the local background intensity of the cluster just before initiation.

Note that the lag time cannot be shorter than the start time of the cluster, giving rise to the dearth of data above slope m=1. Given the start time, there is little correlation with the lag time other than it must be less than the start time. However, we do observe that the majority of LAT condensates occur within the first 120 seconds of the acquisition, a result seen by others.

We also do not observe any strong correlations of lag time with the amount of LAT present before initiation. The ≈100x spread in intensities arises from ≈2x variance in LAT across a single cell, ≈10x variance in LAT expression across cells from a single mouse, ≈5x variance in expression levels across different mouse preps.

Materials and Methods

Tracking Binding Events Under Cells

Spot detection of MCC-Atto647 is relatively straight forward and a number of detection algorithms work well. However, tracking is considerably more difficult. The TCR:pMHC binding events experience a range of velocities, with the fastest binding events occurring at the periphery of the cell and they slow down as the approach the center of the cell. This more linear motion coupled with changing velocity often leads to systematic linking errors. For example, many tracking algorithms prioritize proximity to link spots in one frame to another, but if one spot is moving at a faster velocity then it isn't as straightforward to use distance as a criterion for linking spots. Moreover, the centripetal motion causes the spots to coalesce, leading to multiple merge events. The only solution is to manually inspect each track and only keep those events that have clean linking without a nearby neighbor potentially contaminating the isolation of the binding event. Detection of LAT-eGFP was more difficult due to its relatively small signal over background, especially at the earliest moments of LAT condensation. Again, no automated approach of detection and linking was fully satisfactory, and manual inspection and correction was often necessary. Given these requirements we used TrackMate to facilitate the semi-automated and manual tracking of binding events and intracellular responses (Tinevez et al., 2017).

Constructs, T cell culture, Protein Purification, and other methods

For the exception of the GRB2 and PLC-γ1 constructs all other methods are analogous to previous efforts (Materials and Methods – Chapter 1). Full length human GRB2, which is 99.5% sequence identical to murine GRB2, was a gift from Neel Shah and John Kuriyan, and was cloned into the MSCV plasmid backbone described previously. Full length PLC-γ1 (CloneID:6854923) was purchased from Dharmacon and also cloned into the MSCV backbone.

3 | A Future Direction: Spatially, compositionally, and functionally distinct LAT assemblies.

Introduction

An intriguing result from Chapter 1 "Localized LAT condensation phase transitions discriminate individual TCR:pMHC binding dwell times" was that the number of LAT condensates that formed in response to TCR binding pMHC was supernumerary to the number of binding events. One can frame this result in the following way – if all LAT clusters form as a consequence of the linear signaling chain TCR, LCK, ZAP-70, to LAT, then there must be catalytic amplification of either active TCR or active ZAP coupled with spatial distribution so as to nucleate remote assemblies. The latter has been suggested recently (Katz et al., 2016). The other possibility is that LAT condensates may have alternative origins. A recent study (Raab et al., 2017) has shown that LFA-1 can induce LAT condensates that are enriched in SKAP1. They suggest this occurs via FAK phosphorylation on Y171 of LAT. One study has suggested that LFA-1 can signal through ZAP-70 (Evans et al., 2011). Another alternative origin for LAT clusters has been VAMP7 coated vesicles that create dense deposits of LAT on the membrane (Balagopalan et al., 2018; Larghi et al., 2013). Moreover, there is a long history of TCR and LFA-1 cross-talk (Ardouin et al., 2003; Sedwick et al., 1999; Simonson et al., 2006). Taken together there is evidence that there may be multiple paths to creating LAT condensates that vary in composition and function.

Using the hybrid supported lipid bilayer – live cell platform, we find evidence that there do exist LAT clusters of varying composition, moreover they are spatially distinct. This suggests that LAT can participate in different pathways by forming spatially and compositionally separate signaling centers. Achieving such multifaceted functionality would be difficult for a unified assembly mixing downstream components.

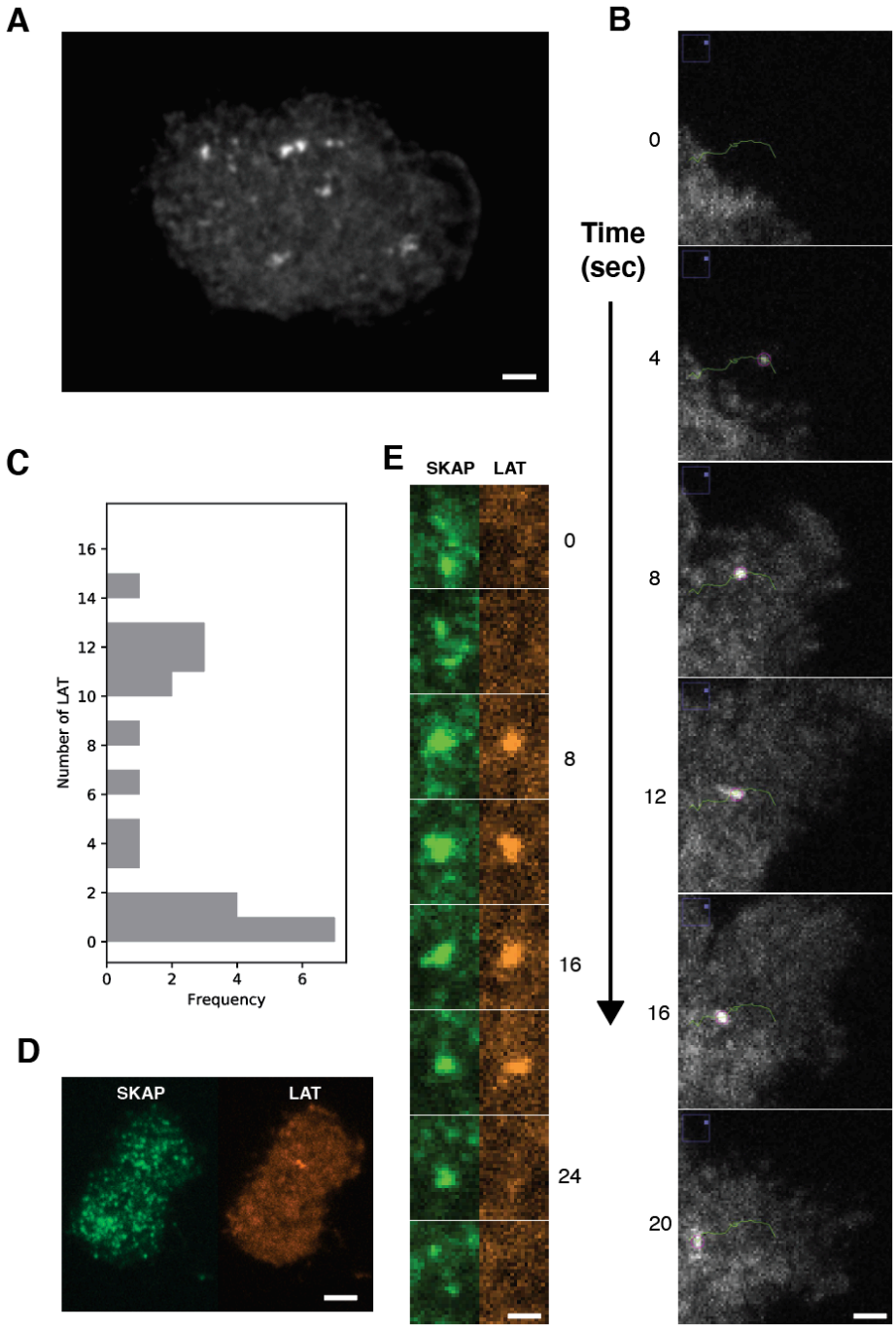

Figure 3-1. LAT clusters on ICAM only are enriched with SKAP1.
Scale bar is 1 µm unless otherwise stated. (A) Soon after deposition onto the bilayer a significant subset of T cells will form multiple LAT clusters. (B) The trajectory of a LAT cluster that is strongly correlated with a lamellipodia extension. Number indicates time elapsed in seconds. (C) The number of LAT clusters counted within 300 seconds of T cell landing on the ICAM bilayer. (D) There are many SKAP puncta present on ICAM only bilayers. Scale bar is 3 µm. (E) SKAP clusters often preceded LAT clusters, but then diminish with them. Number indicates time elapsed in seconds.

ICAM induced LAT clusters are enriched with SKAP1

It was noted previously that few LAT clusters form on ICAM only surfaces. However, this is in comparison to the number of clusters observed relative to pMHC stimulation. After depositing LAT-eGFP transduced T cells onto a his-ICAM only bilayer, a subset of cells produce multiple LAT assemblies (Figure 1A). The number of clusters varies and may be bimodal (Figure 1B). Some of these LAT clusters correlate strongly with lamellipodial extensions (Figure 1C). Given the coupling of LAT to the cytoskeleton through VAV1 (Ardouin et al., 2003; Balagopalan et al., 2010) it is likely that these clusters represent regional decisions to initiate lamellipodial expansion.

Given the previous finding of LFA-1 producing SKAP1 enriched LAT clusters (Raab et al., 2017), we tested whether SKAP1 was present in the ICAM-only induced LAT clusters we observed. Transducing AND T cells with a LAT-eGFP-P2A-SKAP-mScarleti enabled visualization of the localization of both molecules. SKAP has many more noisy puncta than the homogeneous LAT (Figure 1D), however, the co-occurrence of LAT and SKAP in all LAT clusters was clear (Figure 1E). To determine whether SKAP-1 was exclusive to ICAM-only we examine the formation of LAT clusters relative to TCR:pMHC binding. The most common observation was the coincident accumulation of SKAP-1 with LAT condensation (Figure 2). This suggests that SKAP-1 is an integral feature of the LAT assembly.

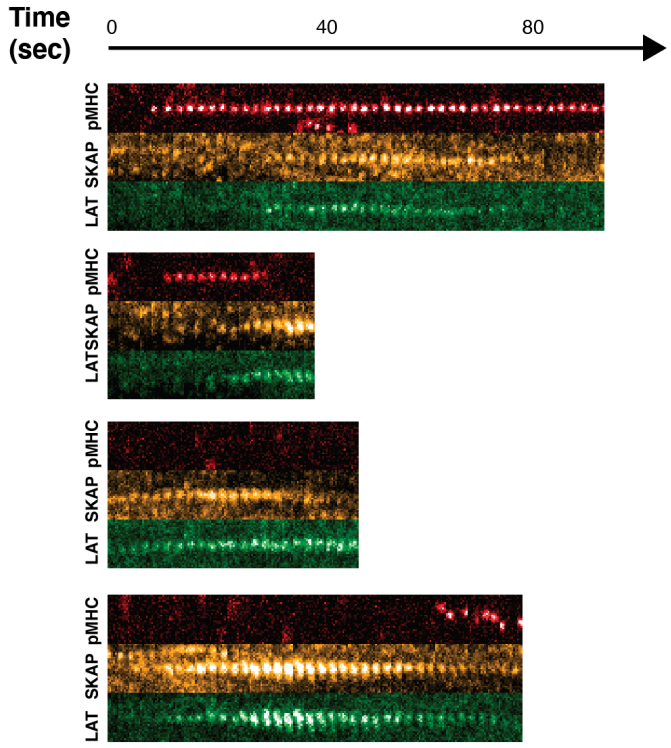

Figure 3-2. SKAP-1 also enriches within LAT clusters formed from pMHC.

Though SKAP-1 and SLP-76 were previously identified to participate in somewhat independent clusters (Raab et al., 2017), our initial results suggest that SKAP-1 may have a more important role in most LAT clusters.

VAMP7 induced LAT density enhancement is orthogonal to pMHC induced LAT condensates.

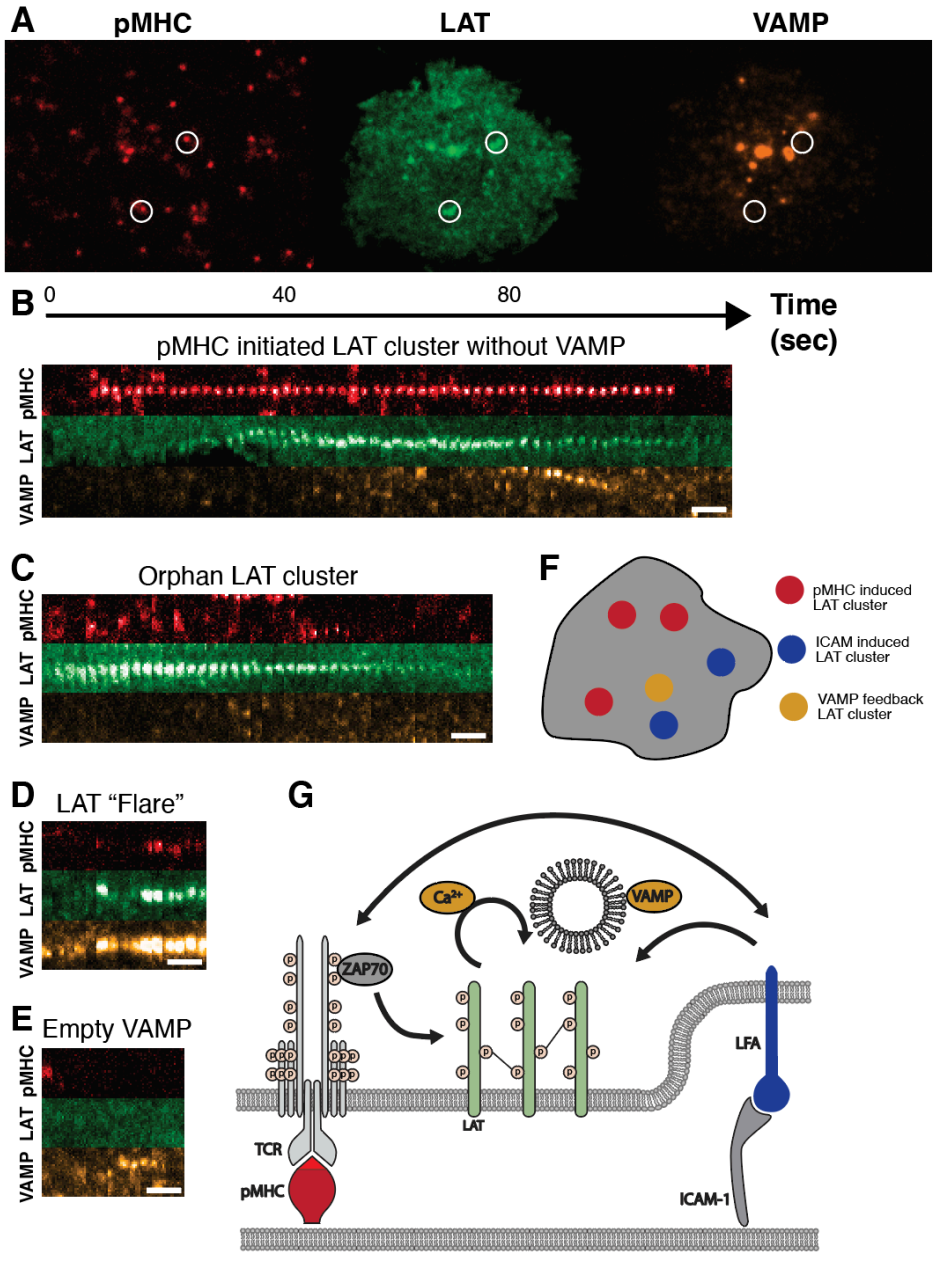

Figure 3-3. VAMP7 induced LAT density enhancement is orthogonal to pMHC induced LAT clusters. (A) Image of entire cell. White circles denote pMHC binding events that successfully colocalize with LAT, but fail to colocalize with VAMP7. (B) Kymograph of pMHC-initiated LAT cluster showing no clear VAMP enrichment. (C) An "orphan" LAT cluster with no observed cause. (D) VAMP7 vesicles can cause a LAT "flare", transient and fluctuates in and out of TIRF. (E) VAMP7 vescicles are also seen to associate with the membrane, but without any observable LAT. (F) Spatially separated LAT clusters processing different information. (G) Schematic of feedback and possible routes to the formation of LAT clusters.

Next, we examined the behavior of VAMP7 vesicle recruitment to the membrane and relative to TCR bound by pMHC (Figure 3A). After landing, VAMP7 recruits to the membrane within 20 seconds. However, the colocalization with LAT is not clear. Most LAT clusters initiated by pMHC show no particular association with VAMP (Figure 3B). In these conditions there is still a significant fraction of orphan LAT clusters (Figure 3C), which may arise from dark pMHC binding, or LFA-1 activation. A new type of LAT event was observed in which LAT-dense VAMP vesicles rapidly enter the TIRF field and may fluctuate before stable association with the membrane (Figure 3D). These patterns of LAT activity is not readily observed for cells only expressing LAT-eGFP and suggests that this may be an artefact of overexpression of VAMP. Finally, there is also observed VAMP vesicles devoid of LAT interacting with the membrane (Figure 3E).

Discussion

The flexible scaffold protein LAT has been implicated in T cell activation (TCR), adhesion (LFA-1), and vesicular feedback (Ca^{2+}, VAMP). However, spatially resolving these potentially different LAT clusters has not been possible. Here we use individual TCR:pMHC binding to sort out the composition of downstream molecules that participate in TCR induced LAT clusters and we spatially distinguish these from other LAT clusters. We find that VAMP7 does not participate in the multimolecular assemblies that follow from TCR:pMHC binding, but it may have a role in later feedback. In addition, SKAP-1 seems to pervade all assemblies of LAT, suggesting the SKAP-1 participates in TCR and LFA-1 cross-talk at the earliest steps in the TCR signal transduction cascade. Many of the SKAP-1 / LAT clusters in the periphery of the cell exhibit a strong correlation with lamellipodial expansion and likely serve as reaction centers catalyzing the expansion. The next steps in this project would be to analyze SLP-76 to see to what extent SLP-76/LAT clusters are independent of SKAP-1/LAT clusters relative to TCR:pMHC bidning.

4 | A Python based course in Biophysics.

Introduction

Much of the way biophysicists interface with their research is through computational analysis. From structure analysis, to simulation, to fitting an exponential curve of fluorescence decay – learning how to do these tasks via computer is essential to gaining competency for research and further inquisition. In the Spring semester of 2019, I had the idea to create a Python based course to teach the thermodynamic and statistical-mechanics material from "The Molecules of Life" (Kuriyan et al., 2012). I pursued this with the helpful guidance from my advisor Jay Groves. These problem sets would also introduce the students to the basics of "running code" and manipulating code to get different results, thereby dramatically increasing their skill set along with their knowledge-base. Python was chosen since it did not need to be licensed, is easy to learn, and is also one of the fastest growing scientific languages.

These problem sets are available open source and free for adaptation as long as credit is given: http://groveslab.cchem.berkeley.edu:8080/dmcaffee/MCBC100A

Below are a list of the problem sets and their aims:

- PS4 2D monatomic gas
    - Show that the Boltzmann distribution is an empirical distribution that arises under the constraints of maximum entropy and conservation of energy.
- PS5 Diatoms, probability, and energy
    - Explore the interplay between energy and entropy (probability)
- PS6 binary phase separation
    - Monte Carlo experiments showing the relationship between exchange energy and phase separation for a 2D lattice.
- PS6 random peptide
    - Generate random peptide polymers and fit to a Freely Jointed Chain model.
- PS8 random switching
    - Examine the statistics of simple processes such as a protein "binding" and "unbinding". A gentle introduction to stochastic processes.
- PS9 stochastic copy number
    - A re-implementation of Van Oudenaarden's classic paper on intrinsic noise in gene regulatory networks (Thattai and van Oudenaarden, 2001).

References

Alfieri, K. (2015). Single Molecule Observations of Receptor: Ligand Binding at Live T Cell-Supported . 74.

Ardouin, L., Bracke, M., Mathiot, A., Pagakis, S.N., Norton, T., Hogg, N., and Tybulewicz, V. (2003). Vav1 transduces TCR signals required for LFA-1 function and cell polarization at the immunological synapse. Eur J Immunol *33*, 790–797.

Au-Yeung, B.B., Shah, N.H., Shen, L., and Weiss, A. (2017). ZAP-70 in Signaling, Biology, and Disease. Annu Rev Immunol *36*, 1–30.

Balagopalan, L., Coussens, N., Sherman, E., Samelson, L., and Sommers, C. (2010). The LAT Story: A Tale of Cooperativity, Coordination, and Choreography. Cold Spring Harbor Perspectives in Biology *2*, a005512 a005512.

Balagopalan, L., Kortum, R.L., Coussens, N.P., Barr, V.A., and Samelson, L.E. (2015). The Linker for Activation of T Cells (LAT) Signaling Hub: From Signaling Complexes to Microclusters. J Biol Chem *290*, 26422–26429.

Balagopalan, L., Yi, J., Nguyen, T., McIntire, K.M., Harned, A.S., Narayan, K., and Samelson, L.E. (2018). Plasma membrane LAT activation precedes vesicular recruitment defining two phases of early T-cell activation. Nat Commun *9*, 2013.

Brameshuber, M., Kellner, F., Rossboth, B.K., Ta, H., Alge, K., Sevcsik, E., Göhring, J., Axmann, M., Baumgart, F., Gascoigne, N.R., et al. (2018). Monomeric TCRs drive T cell antigen recognition. Nat Immunol *19*, 487 496.

Brodovitch, A., Shenderov, E., Cerundolo, V., Bongrand, P., Pierres, A., and van der Merwe, P. (2015). T lymphocytes need less than 3 min to discriminate between peptide MHCs with similar TCR-binding parameters. Eur J Immunol *45*, 1635 1642.

Bunnell, S.C., Hong, D.I., Kardon, J.R., Yamazaki, T., McGlade, J.C., Barr, V.A., and Samelson, L.E. (2002). T cell receptor ligation induces the formation of dynamically regulated signaling assemblies. J Cell Biology *158*, 1263 1275.

Chakraborty, A.K., and Weiss, A. (2014). Insights into the initiation of TCR signaling. Nat Immunol *15*, 798 807.

Chan, A., Irving, Fraser, J., and Weiss, A. (1991). The zeta chain is associated with a tyrosine kinase and upon T-cell antigen receptor stimulation associates with ZAP-70, a

70-kDa tyrosine phosphoprotein. Proc National Acad Sci *88*, 9166–9170.

Chan, G., Kalaitzidis, D., and Neel, B.G. (2008). The tyrosine phosphatase Shp2 (PTPN11) in cancer. Cancer Metast Rev *27*, 179–192.

Cognet, L., Leduc, C., and Lounis, B. (2014). Advances in live-cell single-particle tracking and dynamic super-resolution imaging. Current Opinion in Chemical Biology *20*, 78 85.

Cole, D.K., Pumphrey, N.J., Boulter, J.M., Sami, M., Bell, J.I., Gostick, E., Price, D.A., Gao, G.F., Sewell, A.K., and Jakobsen, B.K. (2007). Human TCR-Binding Affinity is Governed by MHC Class Restriction. J Immunol *178*, 5727–5734.

Cordoba, S.-P.P., Choudhuri, K., Zhang, H., Bridge, M., Basat, A.B., Dustin, M.L., and van der Merwe, P. (2013). The large ectodomains of CD45 and CD148 regulate their segregation from and inhibition of ligated T-cell receptor. Blood *121*, 4295–4302.

Corr, M., Slanetz, A., Boyd, L., Jelonek, M., Khilko, S., al-Ramadi, B., Kim, Y., Maher, S., Bothwell, A., and Margulies, D. (1994). T cell receptor-MHC class I peptide interactions: affinity, kinetics, and specificity. Science *265*, 946–949.

Cruz-Orcutt, N., Vacaflores, A., Connolly, S.F., Bunnell, S.C., and Houtman, J. (2014). Activated PLC-γ1 is catalytically induced at LAT but activated PLC-γ1 is localized at both LAT- and TCR-containing complexes. Cellular Signalling *26*, 797 805.

Daniels, M.A., Teixeiro, E., Gill, J., Hausmann, B., Roubaty, D., Holmberg, K., Werlen, G., Holländer, G.A., Gascoigne, N.R., and Palmer, E. (2006). Thymic selection threshold defined by compartmentalization of Ras/MAPK signalling. Nature *444*, 724 729.

Davis, S.J., and van der Merwe, A.P. (2006). The kinetic-segregation model: TCR triggering and beyond. Nature Immunology *7*, 803–809.

Delon, J., Bercovici, N., Raposo, G., Liblau, R., and Trautmann, A. (1998). Antigen-dependent and -independent Ca 2+ Responses Triggered in T Cells by Dendritic Cells Compared with B Cells. J Exp Medicine *188*, 1473–1484.

Demotz, S., Grey, H., and Sette, A. (1990). The minimal number of class II MHC-antigen complexes needed for T cell activation. Science *249*, 1028–1030.

Douglass, A.D., and Vale, R.D. (2005). Single-Molecule Microscopy Reveals Plasma Membrane Microdomains Created by Protein-Protein Networks that Exclude or Trap Signaling Molecules in T Cells. Cell *121*, 937–950.

Dunn, K., Kamocka, M., and nald, J. (2011). A practical guide to evaluating colocalization in biological microscopy. Am J Physiology - Cell Physiology *300*, C723 C742.

Dustin, M.L., and Baldari, C.T. (2017). The Immune Synapse: Past, Present, and Future. T-Cell Development *1584*, 1 5.

Ebert, P.J., Jiang, S., Xie, J., Li, Q.-J., and vis, M. (2009). An endogenous positively selecting peptide enhances mature T cell responses and becomes an autoantigen in the absence of microRNA miR-181a. Nature Immunology *10*, ni.1797.

von Essen, M., Kongsbak, M., Schjerling, P., Olgaard, K., Ødum, N., and Geisler, C. (2010). Vitamin D controls T cell antigen receptor signaling and activation of human T cells. Nat Immunol *11*, 344 349.

Evans, R., Lellouch, A.C., Svensson, L., wall, A., and Hogg, N. (2011). The integrin LFA-1 signals through ZAP-70 to regulate expression of high-affinity LFA-1 on T lymphocytes. Blood *117*, 3331–3342.

Fortanet, J., Chen, C., Chen, Y.-N.P., Chen, Z., Deng, Z., Firestone, B., Fekkes, P., Fodor, M., Fortin, P.D., Fridrich, C., et al. (2016). Allosteric Inhibition of SHP2: Identification of a Potent, Selective, and Orally Efficacious Phosphatase Inhibitor. J Med Chem *59*, 7773–7782.

Gaud, G., Lesourne, R., and Love, P.E. (2018). Regulatory mechanisms in T cell receptor signalling. Nat Rev Immunol *18*, 485–497.

Ge, H., Qian, M., and Qian, H. (2012). Stochastic theory of nonequilibrium steady states. Part II: Applications in chemical biophysics. Phys Reports *510*, 87 118.

Germain, R.N. (2010). Computational analysis of T cell receptor signaling and ligand discrimination – Past, present, and future. Febs Lett *584*, 4814–4822.

Harding, C.V., and Unanue, E.R. (1990). Quantitation of antigen-presenting cell MHC class II/peptide complexes necessary for T-cell stimulation. Nature *346*, 574–576.

Hopfield, J. (1974). Kinetic proofreading: a new mechanism for reducing errors in biosynthetic processes requiring high specificity. Proc National Acad Sci *71*, 4135–4139.

Houtman, J.C., Higashimoto, Y., Dimasi, N., Cho, S., Yamaguchi, H., Bowden, B., Regan, C., Malchiodi, E.L., Mariuzza, R., Schuck, P., et al. (2004). Binding Specificity of Multiprotein Signaling Complexes Is Determined by Both Cooperative Interactions and Affinity Preferences †. Biochemistry-Us *43*, 4170 4178.

Houtman, J.C., Yamaguchi, H., Barda-Saad, M., Braiman, A., Bowden, B., Appella, E., Schuck, P., and Samelson, L.E. (2006). Oligomerization of signaling complexes by the multipoint binding of GRB2 to both LAT and SOS1. Nature Structural & Molecular

Biology *13*, 798 805.

Huang, J., Brameshuber, M., Zeng, X., Xie, J., Li, Q., Chien, Y., Valitutti, S., and vis, M. (2013). A Single Peptide-Major Histocompatibility Complex Ligand Triggers Digital Cytokine Secretion in CD4+ T Cells. Immunity *39*, 846 857.

Huang, W.Y., Yan, Q., Lin, W.-C., Chung, J.K., Hansen, S.D., Christensen, S.M., Tu, H.-L., Kuriyan, J., and Groves, J.T. (2016). Phosphotyrosine-mediated LAT assembly on membranes drives kinetic bifurcation in recruitment dynamics of the Ras activator SOS. Proceedings of the National Academy of Sciences *113*, 8218 8223.

Huang, W.Y., Ditlev, J.A., Chiang, H.-K., Rosen, M.K., and Groves, J.T. (2017a). Allosteric Modulation of Grb2 Recruitment to the Intrinsically Disordered Scaffold Protein, LAT, by Remote Site Phosphorylation. J Am Chem Soc *139*.

Huang, W.Y., Chiang, H.-K., and Groves, J.T. (2017b). Dynamic Scaling Analysis of Molecular Motion within the LAT:Grb2:SOS Protein Network on Membranes. Biophysical Journal *113*, 1807 1813.

Huse, M., Klein, L.O., Girvin, A.T., Faraj, J.M., Li, Q., Kuhns, M.S., and vis, M. (2007). Spatial and temporal dynamics of T cell receptor signaling with a photoactivatable agonist. Immunity *27*, 76 88.

Iezzi, G., Karjalainen, K., and Lanzavecchia, A. (1998). The Duration of Antigenic Stimulation Determines the Fate of Naive and Effector T Cells. Immunity *8*, 89–95.

Ilienko, A. (2013). Continuous counterparts of Poisson and binomial distributions and their properties.

Irvine, D.J., Purbhoo, M.A., Krogsgaard, M., and vis, M. (2002). Direct observation of ligand recognition by T cells. Nature *419*, 845 849.

Iwashima, M., Irving, van Oers, N., Chan, A., and Weiss, A. (1994). Sequential interactions of the TCR with two distinct cytoplasmic tyrosine kinases. Science (New York, N.Y.) *263*, 1136–1139.

Katz, Z.B., Novotná, L., Blount, A., and Lillemeier, B.F. (2016). A cycle of Zap70 kinase activation and release from the TCR amplifies and disperses antigenic stimuli. Nat Immunol *18*, 86 95.

Klammt, C., Novotná, L., Li, D.T., Wolf, M., Blount, A., Zhang, K., Fitchett, J.R., and Lillemeier, B.F. (2015). T cell receptor dwell times control the kinase activity of Zap70. Nat Immunol *16*, 961 969.

Kortum, R.L., Balagopalan, L., Alexander, C.P., Garcia, J., Pinski, J.M., Merrill, R.K., Nguyen, P.H., Li, W., Agarwal, I., Akpan, I.O., et al. (2013). The Ability of Sos1 to Oligomerize the Adaptor Protein LAT Is Separable from Its Guanine Nucleotide Exchange Activity in Vivo. Sci Signal *6*, ra99–ra99.

Kuriyan, J., Konforti, B., and Wemmer, D. (2012). The Molecules of Life: Physical and Chemical Principles.

Larghi, P., Williamson, D.J., Carpier, J.-M., Dogniaux, S., Chemin, K., Bohineust, A., Danglot, L., Gaus, K., Galli, T., and Hivroz, C. (2013). VAMP7 controls T cell activation by regulating the recruitment and phosphorylation of vesicular Lat at TCR-activation sites. Nature Immunology *14*, 723 731.

Li, P., Banjade, S., Cheng, H.-C., Kim, S., Chen, B., Guo, L., Llaguno, M., Hollingsworth, J.V., King, D.S., Banani, S.F., et al. (2012). Phase transitions in the assembly of multivalent signalling proteins. Nature *483*, 336 340.

Lin, J.J., Low-Nam, S.T., Alfieri, K.N., McAffee, D.B., Fay, N.C., and Groves, J.T. (2019). Mapping the stochastic sequence of individual ligand-receptor binding events to cellular activation: T cells act on the rare events. Sci Signal *12*, eaat8715.

Liu, Z., Chen, O., Wall, B.J., Zheng, M., Zhou, Y., Wang, L., Vaseghi, H., Qian, L., and Liu, J. (2017). Systematic comparison of 2A peptides for cloning multi-genes in a polycistronic vector. Sci Rep-Uk *7*, 2193.

Lo, W.-L., Shah, N.H., Ahsan, N., Horkova, V., Stepanek, O., Salomon, A.R., Kuriyan, J., and Weiss, A. (2018). Lck promotes Zap70-dependent LAT phosphorylation by bridging Zap70 to LAT. Nat Immunol *19*, 733 741.

Lo, W.-L., Shah, N.H., Rubin, S.A., Zhang, W., Horkova, V., Fallahee, I.R., Stepanek, O., Zon, L.I., Kuriyan, J., and Weiss, A. (2019). Slow phosphorylation of a tyrosine residue in LAT optimizes T cell ligand discrimination. Nat Immunol *20*, 1481–1493.

Macian, F. (2005). NFAT proteins: key regulators of T-cell development and function. Nat Rev Immunol *5*, 472–484.

Manna, A., Zhao, H., Wada, J., Balagopalan, L., Tagad, H.D., Appella, E., Schuck, P., and Samelson, L.E. (2018). Cooperative assembly of a four-molecule signaling complex formed upon T cell antigen receptor activation. Proc National Acad Sci *115*, 201817142.

Manz, B.N., Jackson, B.L., Petit, R.S., Dustin, M.L., and Groves, J. (2011). T-cell triggering thresholds are modulated by the number of antigen within individual T-cell receptor clusters. Proceedings of the National Academy of Sciences *108*, 9089–9094.

Matsui, K., Boniface, J., Steffner, P., Reay, P., and vis, M. (1994). Kinetics of T-cell receptor binding to peptide/I-Ek complexes: correlation of the dissociation rate with T-cell responsiveness. Proc National Acad Sci *91*, 12862 12866.

McKeithan, T. (1995). Kinetic proofreading in T-cell receptor signal transduction. Proc National Acad Sci *92*, 5042 5046.

Mutch, S.A., Fujimoto, B.S., Kuyper, C.L., Kuo, J.S., Bajjalieh, S.M., and Chiu, D.T. (2007). Deconvolving Single-Molecule Intensity Distributions for Quantitative Microscopy Measurements. Biophysical Journal *92*, 2926 2943.

Ninio, J. (1975). Kinetic amplification of enzyme discrimination. Biochimie *57*, 587 595.

Nye, J.A., and Groves, J.T. (2008). Kinetic Control of Histidine-Tagged Protein Surface Density on Supported Lipid Bilayers. Langmuir Acs J Surfaces Colloids *24*, 4145 4149.

O'Donoghue, G.P., Pielak, R.M., Smoligovets, A.A., Lin, J.J., and Groves, J.T. (2013a). Direct single molecule measurement of TCR triggering by agonist pMHC in living primary T cells. Elife *2*, e00778.

O'Donoghue, G.P., Pielak, R.M., Smoligovets, A.A., Lin, J.J., and Groves, J.T. (2013b). Direct single molecule measurement of TCR triggering by agonist pMHC in living primary T cells. ELife *2013*, 1–16.

Park, D., Rho, H., and Rhee, S. (1991). CD3 stimulation causes phosphorylation of phospholipase C-gamma 1 on serine and tyrosine residues in a human T-cell line. Proc National Acad Sci *88*, 5453–5456.

Pielak, R.M., O'Donoghue, G.P., Lin, J.J., Alfieri, K.N., Fay, N.C., Low-Nam, S.T., and Groves, J.T. (2017). Early T cell receptor signals globally modulate ligand:receptor affinities during antigen discrimination. Proc National Acad Sci *114*, 12190 12195.

Podtschaske, M., Benary, U., Zwinger, S., Höfer, T., Radbruch, A., and Baumgrass, R. (2007). Digital NFATc2 Activation per Cell Transforms Graded T Cell Receptor Activation into an All-or-None IL-2 Expression. Plos One *2*, e935.

Raab, M., Lu, Y., Kohler, K., Smith, X., Strebhardt, K., and Rudd, C.E. (2017). LFA-1 activates focal adhesion kinases FAK1/PYK2 to generate LAT-GRB2-SKAP1 complexes that terminate T-cell conjugate formation. Nature Communications *8*, 16001.

Reay, P., Kantor, R., and Davis, M. (1994). Use of global amino acid replacements to define the requirements for MHC binding and T cell recognition of moth cytochrome c (93-103). Journal of Immunology (Baltimore, Md. : 1950) *152*, 3946–57.

Robert, P., Aleksic, M., Dushek, O., Cerundolo, V., Bongrand, P., and van der Merwe, A.P. (2012). Kinetics and Mechanics of Two-Dimensional Interactions between T Cell Receptors and Different Activating Ligands. Biophys J *102*, 248–257.

Rojas, M., Restrepo-Jiménez, P., Monsalve, D.M., Pacheco, Y., Acosta-Ampudia, Y., Ramírez-Santana, C., Leung, P., Ansari, A.A., Gershwin, E.M., and Anaya, J.-M. (2018). Molecular mimicry and autoimmunity. J Autoimmun *95*, 100–123.

Rosette, C., Werlen, G., Daniels, M.A., Holman, P.O., Alam, S.M., Travers, P.J., Gascoigne, N., Palmer, E., and Jameson, S.C. (2001). The Impact of Duration versus Extent of TCR Occupancy on T Cell Activation A Revision of the Kinetic Proofreading Model. Immunity *15*, 59–70.

Rossboth, B., Arnold, A.M., Ta, H., Platzer, R., Kellner, F., Huppa, J.B., Brameshuber, M., Baumgart, F., and Schütz, G.J. (2018). TCRs are randomly distributed on the plasma membrane of resting antigen-experienced T cells. Nat Immunol *19*, 1 12.

Sedwick, C., Morgan, M., Jusino, L., Cannon, J., Miller, J., and Burkhardt, J. (1999). TCR, LFA-1, and CD28 play unique and complementary roles in signaling T cell cytoskeletal reorganization. J Immunol Baltim Md 1950 *162*, 1367–1375.

Shah, N.H., Wang, Q., Yan, Q., Karandur, D., Kadlecek, T.A., Fallahee, I.R., Russ, W.P., Ranganathan, R., Weiss, A., and Kuriyan, J. (2016). An electrostatic selection mechanism controls sequential kinase signaling downstream of the T cell receptor. Elife *5*, e20105.

Sherman, E., Barr, V.A., Merrill, R.K., Regan, C.K., Sommers, C.L., and Samelson, L.E. (2016). Hierarchical nanostructure and synergy of multimolecular signalling complexes. Nature Communications *7*, 12161.

Siller-Farfán, J.A., and Dushek, O. (2018). Molecular mechanisms of T cell sensitivity to antigen. Immunol Rev *285*, 194–205.

Simonson, W.T., Franco, S.J., and Huttenlocher, A. (2006). Talin1 Regulates TCR-Mediated LFA-1 Function. J Immunol *177*, 7707–7714.

Štefanová, I., Hemmer, B., Vergelli, M., Martin, R., Biddison, W.E., and Germain, R.N. (2003). TCR ligand discrimination is enforced by competing ERK positive and SHP-1 negative feedback pathways. Nat Immunol *4*, 248 254.

Stepanek, O., Prabhakar, A.S., Osswald, C., King, C.G., Bulek, A., Naeher, D., Beaufils-Hugot, M., Abanto, M.L., Galati, V., Hausmann, B., et al. (2014). Coreceptor scanning by the T cell receptor provides a mechanism for T cell tolerance. Cell *159*, 333 345.

Su, X., Ditlev, J.A., Hui, E., Xing, W., Banjade, S., Okrut, J., King, D.S., Taunton, J., Rosen,

M.K., and Vale, R.D. (2016). Phase separation of signaling molecules promotes T cell receptor signal transduction. Science *352*, 595 599.

Sukenik, S., Frushicheva, M.P., Waknin-Lellouche, C., Hallumi, E., Ifrach, T., Shalah, R., Beach, D., Avidan, R., Oz, I., Libman, E., et al. (2017). Dimerization of the adaptor Gads facilitates antigen receptor signaling by promoting the cooperative binding of Gads to the adaptor LAT. Sci Signal *10*, eaal1482.

Thattai, M., and van Oudenaarden, A. (2001). Intrinsic noise in gene regulatory networks. Proc National Acad Sci *98*, 8614 8619.

Tinevez, J.-Y., Perry, N., Schindelin, J., Hoopes, G.M., Reynolds, G.D., Laplantine, E., Bednarek, S.Y., Shorte, S.L., and Eliceiri, K.W. (2017). TrackMate: An open and extensible platform for single-particle tracking. Methods *115*, 80–90.

Tischer, D.K., and Weiner, O. (2019). Light-based tuning of ligand half-life supports kinetic proofreading model of T cell signaling. Elife *8*, e42498.

Velazquez, C., DiPaolo, R., and Unanue, E.R. (2001). Quantitation of Lysozyme Peptides Bound to Class II MHC Molecules Indicates Very Large Differences in Levels of Presentation. J Immunol *166*, 5488–5494.

Williamson, D.J., Owen, D.M., Rossy, J., Magenau, A., Wehrmann, M., Gooding, J.J., and Gaus, K. (2011). Pre-existing clusters of the adaptor Lat do not participate in early T cell signaling events. Nature Immunology *12*, 655 662.

Wucherpfennig, K.W., and Strominger, J.L. (1995). Molecular mimicry in T cell-mediated autoimmunity: Viral peptides activate human T cell clones specific for myelin basic protein. Cell *80*, 695–705.

Yi, J., Balagopalan, L., Nguyen, T., McIntire, K.M., and Samelson, L.E. (2019). TCR microclusters form spatially segregated domains and sequentially assemble in calcium-dependent kinetic steps. Nat Commun *10*, 277.

Zhang, W., Sloan-Lancaster, J., Kitchen, J., Trible, R., and Samelson, L. (1998). LAT The ZAP-70 Tyrosine Kinase Substrate that Links T Cell Receptor to Cellular Activation. Cell *92*, 83–92.